Imaging of Underground Structure Using HAARP

Randall L. Mackie

GSY-USA, Inc
2261 Market St, PMB 643
San Francisco, CA 94115-1600
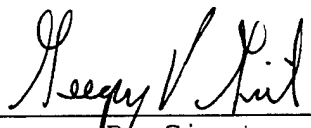
February 1999

Final Report
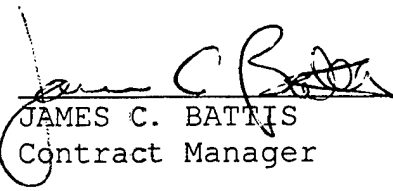
AIR FORCE RESEARCH LABORATORY
Space Vehicles Directorate
29 Randolph Rd
AIR FORCE MATERIEL COMMAND
Hanscom AFB, MA 01731-3010

20020124 421

"This technical report has been reviewed and is approved for publication"

JAMES C. BATTIS
Contract Manager

Gregory P. Ginet
Branch Chief

REPORT DOCUMENTATION PAGE

Form Approved
OMB No. 0704-0188

Public reporting burden for this collection of information is estimated to average 1 hour per response, including the time for reviewing instructions, searching existing data sources, gathering and maintaining the data needed, and completing and reviewing the collection of information. Send comments regarding this burden estimate or any other aspect of this collection of information, including suggestions for reducing this burden, to Washington Headquarters Services, Directorate for Information Operations and Reports, 1215 Jefferson Davis Highway, Suite 1204, Arlington, VA 22202-4302, and to the Office of Management and Budget, Paperwork Reduction Project (0704-0188), Washington, DC 20503.

1. AGENCY USE ONLY *(Leave blank)*	2. REPORT DATE	3. REPORT TYPE AND DATES COVERED
	March, 1999	Final Report

4. TITLE AND SUBTITLE
Imaging of Underground Structure Using HAARP

6. AUTHOR(S)
Randall L. Mackie

5. FUNDING NUMBERS
PE 63160D
PR 4268
TA SD
WU AB
C-F19628-98-C-0016

7. PERFORMING ORGANIZATION NAME(S) AND ADDRESS(ES)
GSY-USA, Inc.
2261 Market St., PMB 643
San Francisco, CA
94114-1600

8. PERFORMING ORGANIZATION REPORT NUMBER

GSY-99/001

9. SPONSORING/MONITORING AGENCY NAME(S) AND ADDRESS(ES)
Air Force Research Laboratory
Hanscom Air Force Base, Massachusetts
01731-3010
Contract Manager James Battis

10. SPONSORING/MONITORING AGENCY REPORT NUMBER

AFRL-VS-TR-1999-1511

11. SUPPLEMENTARY NOTES

12a. DISTRIBUTION AVAILABILITY STATEMENT
Approved for Public Release; distribution unlimited

12b. DISTRIBUTION CODE

13. ABSTRACT *(Maximum 200 words)*
Non-invasive imaging of underground structure is important for the detection of hidden tunnels and other hazards, as well as resource exploration, mineral exploration, and environmental contamination problems. We processed and analyzed electromagnetic imaging data sets provided by the Air Force Research Laboratory (AFRL). The main parts of this study included: 1) subsurface imaging using smooth minimum-structure algorithms, 2) adaptation of imaging algorithms for parametric inversions, 3) analysis of the sensitivity and resolution of data to subsurface features and sharp boundaries, and 4) modification of robust processing algorithms for AMT data. Our analysis using synthetic data for simple models indicates that subsurface tunnels can be successfully detected if they are at a depth to diameter ratio of approximately 3:1 or less. Detection of tunnels in actual field conditions is more difficult because of the low signal levels in the AMT frequency range and geologic noise. This was evident in all data sets analyzed under this contract. The HAARP transmitter has the potential to be a valuable exploration tool in that it could generate EM fields that appeared locally as plane waves and could overcome the problems with low AMT signal levels and geologic noise. Our modifications to robust processing algorithms for AMT data and for controlled source data have proven useful for analyzing data with low signal levels and large amounts of noise.

14. SUBJECT TERMS
HAARP
Electromagnetics
Inversion

15. NUMBER OF PAGES
43

16. PRICE CODE

17. SECURITY CLASSIFICATION OF REPORT	18. SECURITY CLASSIFICATION OF THIS PAGE	19. SECURITY CLASSIFICATION OF ABSTRACT	20. LIMITATION OF ABSTRACT
UNCLASSIFIED	UNCLASSIFIED	UNCLASSIFIED	UNL

Standard Form 298 (Rev. 2-89) (EG)
Prescribed by ANSI Std. 239.18
Designed using Perform Pro, WHS/DIOR, Oct 94

Contents

List of Figures

1. Summary

Under the auspices of a one year contract with the Air Force Research Laboratory, research was conducted on advanced imaging of underground structures using artificial electromagnetic sources such as the High frequency Active Auroral Research Program (HAARP) Ionospheric Research Instrument. Non-invasive imaging of underground structure is important for the detection of hidden tunnels and other hazards, as well as resource exploration, mineral exploration, and environmental contamination problems. Under this contract, we explored the following areas related to underground tunnel detection: 1) imaging algorithms including minimum structure inversions and parametric inversions, 2) analysis of the sensitivity and resolution of surface electromagnetic data to subsurface tunnels, 3) analysis of data collected over known tunnel structures, both by the US Geological Survey and by APTI, Inc., and 4) modification of our robust processing algorithms to deal with AMT data and for controlled source data.

While our minimum structure imaging codes had previously been written and tested, we developed new imaging codes that performed parametric inversions, which are inversions for simple geometric models rather than fully inhomogenous models. Two such codes were developed, one that inverted data for sharp boundaries, and one that inverted data for a rectangular tunnel in a homogeneous background media. These inversion algorithms are useful for testing the possible classes of models consistent with a given set of data. The imaging algorithms, along with simple forward modeling, were used to examine the sensitivity and resolution of surface EM data to subsurface tunnels. Our analysis indicated that tunnels needed to be at approximately a depth to diameter ratio of 3:1 or less to be resolvable. Actual field data collected over known tunnels showed that in a realistic situation, however, that even this may be difficult to obtain because of low AMT signal levels, and geologic noise. A phased array transmitter similar to HAARP was used in one test across the Silver Fox mine in Alaska, but the usefulness of the transmitter in this situation was limited at best. Higher power transmitters will likely be more useful. Finally, our robust processing algorithms have been adapted to deal with some of the problems with AMT data and controlled sources, and they show considerable promise for future work.

2. Introduction

Non-invasive imaging of natural and man-made underground structure continues to be an important issue in natural resource exploration (oil, gas, minerals, and geothermal), environmental contamination, and underground hazards detection (tunnels and unexploded ordnance, for example). Sub-surface imaging can be accomplished using a variety of geophysical data such as seismic, gravity, magnetic, and electrical measurements. In particular, electrical geophysical techniques (e.g., d.c. resistivity, magnetotellurics, and electromagnetic (EM) soundings) are valuable in subsurface exploration because the bulk electrical conductivity of the subsurface is diagnostic of parameters such as the amount and connectivity of pore fluids, the presence of voids, the presence of chemical contaminants, and the presence of anomalously conductive fluids. Even when they do not directly detect the presence of fluids, contaminants, or voids, electrical methods can provide valuable information on structural parameters and soil properties. For example, an image of the sub-surface electrical conductivity can be related to geologic and structural features that would indicate oil and gas deposits and therefore be useful information for resource exploration.

Perhaps one of the most common and widely used of electrical geophysical methods is the exploration method known as magnetotellurics (MT) (Vozoff, 1991). In the MT method, measurements of the naturally-occurring electric and magnetic fields at earth's surface are used to image the subsurface electrical conductivity. The frequency range spanned by MT measurements is typically from 500-0.001 Hz, but sometimes higher frequency measurements are made up to 20,000 Hz in the method known as audio-frequency MT, or AMT. Recent advances in hardware and MT data processing, modeling, and interpretation have led to many successes in crustal geologic and geophysical exploration. Nonetheless, MT still suffers from certain inherent limitations including low signal strength in the 1.0 to 0.1 Hz region ('dead-band') and around 1 to 2 kHz (the AMT dead-band), variable signal levels, and man-made electrical noise that obscures the natural field variations and leads to poor data quality.

To overcome these limitations, geophysicists have employed artificial sources to generate large amplitude EM fields that can be measured in a manner similar to the traditional MT method. This technique, a variant of the MT method, is known as controlled-source MT (CSMT), and the sources are typically long grounded dipoles or large loops of wires that are

energized with alternating currents to induce EM fields in the earth. CSMT methods overcome the problems with low signal levels, noise, and the dead-band, but unless very large sources and field generators are used, the penetration depths for CSMT are limited to a few kilometers at best. Additionally, computer simulations of EM fields in a heterogeneous earth for finite sources such as grounded dipoles is time-consuming and computationally intensive, whereas modeling EM fields from a plane wave source, such as in the MT method, is much quicker and less computationally-intensive. Even though geophysicists often go to great lengths in CSMT surveys to approximate plane wave fields (e.g., making measurements far away from the source), there are always source effects in the measurements that can make CSMT data difficult to interpret.

Therefore, a controllable EM source that could generate signals that *appeared* locally as plane waves and whose signals were significantly stronger than background levels would be of special interest for subsurface imaging since it would overcome the limitations of the traditional MT and CSMT methods. The phased array radio transmitter of the High frequency Active Auroral Research Program (HAARP) has the potential to be just such a controlled plane-wave source. By controlling the modulation frequency of the transmitter, which was originally designed for upper atmospheric and solar-terrestrial research, EM waves can be generated at the frequencies needed for geophysical exploration of the shallow subsurface. However, the transmitted power levels that are presently sustainable at the HAARP facility, which is only in the development phase of its construction, are much lower than the power levels planned when future phases are complete. Consequently, the transmitted signals are only observable within the near vicinity of the facility, but when at full power, it is possible that the transmitted signals will be sufficiently strong to be used for exploration and imaging at greater distances.

The potential advantage of using a source like the HAARP transmitter is that since the observed signals would appear locally as plane waves, one could use the much simpler and faster analysis and modeling codes developed for the MT method and not have to worry about the effects of finite-dimension sources. Additionally, EM waves generated by the HAARP transmitters would not suffer from the 'dead-band' limitations of the MT natural fields, and in fact may allow the collection of interpretable data even in areas with high levels of man-made electrical noise. Finally, since the HAARP transmitters have the potential to generate EM waves at low frequencies, one can explore deeper crustal structure that are not accessible to the usual

3

CSMT sources. The viability of using the HAARP transmitters as a controlled-source geophysical exploration tool has already been demonstrated (MacEnany, 1997, personal communication) in tests carried out by Advanced Power Technologies, Inc. (APTI) for underground tunnel detection.

In this report, we summarize research carried out on the applicability of using HAARP for underground tunnel detection. First, we outline the general concepts behind our imaging algorithms and extension to parametric models. Second, we discuss the sensitivity of EM measurements to underground tunnels using simple synthetic models and two-dimensional modeling and inversion algorithms. Third, we present an analysis of data collected by the both the US Geological Survey and APTI over known tunnel structures. Finally, we summarize our recent advances with robust processing codes.

3. Inversion Algorithms

The goal of EM imaging (also known as tomography or inversion) is to infer the electrical conductivity of the earth's subsurface on the basis of measurements of the electric and magnetic fields at the surface or in boreholes. The problem can be expressed as an inverse problem of the form

$$d = A(m) + e.$$

The data vector d has the apparent resistivities and phases for the TM and/or TE modes for all frequencies and locations. The resistivity of the earth is parameterized by a model vector m, A is a functional that predicts the theoretical value of d for a particular m, and e is the observational error in d. In general, the earth's resistivity (ρ) varies significantly both vertically and laterally. Therefore, it is appropriate to consider m to be a function of 3-D position. However, owing to the computational demands of 3-D model simulations and because 2-D approximations are often adequate, in this report we will consider m to be a function of 2-D position. To enforce positivity ($\rho > 0$) it is convenient to let m be the logarithm of ρ. For numerical implementation, the model function m is discretized in terms of a 2-D grid of rectangular blocks.

The functional A is defined implicitly by Maxwell's equations. At MT frequencies, conduction currents dominate over displacement currents. Thus, the physical process is one of EM induction, with EM fields diffusing through the conductive earth rather than propagating as

EM waves. Except for simple classes of resistivity models, it is necessary to solve Maxwell's equations numerically. Numerical techniques applied to the MT problem include Madden's (1972) transmission network method, the finite difference method (Mackie et al., 1994), and finite element method (Wannamaker et al, 1984), among others.

The main problem with electromagnetic tomography is that it is a very ill-posed inverse problem. Electromagnetic measurements can be made only at a finite number of locations (surface or borehole), whereas the conductivity of subsurface materials is a function of position which can vary strongly in all three dimensions and therefore has an infinite number of degrees of freedom. Moreover, the inverse problem is strongly nonlinear and it is not possible to "back-project" or migrate the data directly into a meaningful image of the subsurface, as is done with seismic reflection data. An iterative process is therefore necessary. Finally, the fact that the EM waves diffuse through the media rather than propagate as waves limits the basic information content of the data.

3.1 Minimum structure inversion

Because of the ill-posedness of the EM inverse problem, it must be stabilized by applying regularization techniques. Our 2-D MT inversion algorithm is based on the method of Tikhonov regularization (Tikhonov and Arsenin, 1977). This method defines a 'regularized solution' of the inverse problem as a model that minimizes an objective functional of the form

$$\Phi = \sum (d - A(m))^2 / \sigma^2 + \tau \, S(m) \, .$$

Here, τ is a positive number known as the 'regularization parameter'. The first term of Φ is a weighted error sum of squares ('misfit') for the model m. For each datum, σ is the standard deviation of the error e. The second term is τ times a functional, $S(m)$, known as the 'stabilizing functional'.

There is no consensus in the geophysical community about the best choice of the stabilizing functional, S. Some workers, motivated by a stochastic inversion framework (e.g. Tarantola, 1987), define S in terms of a prior model, m_o, and prior covariance operator, R_{mm}. This approach has been taken by Park and Van (1991) and Zhang et al (1995) in the 3D d.c. resistivity problem. Alternatively, many workers choose S as a measure of the spatial roughness

5

of *m*, which is typically associated with the size of its first or second spatial derivatives. The motivation in this case is to find the simplest explanation of the data in the form of models with minimum structure (Constable et al, 1987; Smith and Booker, 1988; Rodi, 1989). The minimum structure approach has been used in 3D resistivity by Ellis and Oldenburg (1994), while several workers have employed it in electromagnetic inversion problems (Jiracek et al, 1987; deGroot-Hedlin and Constable, 1990; Smith and Booker, 1991; Newman, 1995). However, the precise definition of *S* differs among the workers who have taken this approach.

Our current tomography algorithm provides different options for the stabilizing functional, but in general we have found a very simple functional involving only second derivatives of *m* to be effective:

$$S(m) = \int (\nabla^2 m)^2 \, dx$$

where ∇^2 denotes the Laplacian operator. We point out that one cannot take for granted that the minimization of Φ is well-posed for any choice of stabilizing functional. Unless *S* constrains derivatives of *m* of sufficiently high order, numerical solutions of the inverse problem will depend strongly on the model discretization (grid) and the model will contain grid artifacts regardless of how fine the grid is. Numerical experiments we have performed show evidence of this.

Another reason for choosing minimum structure algorithms is related to the physical process that controls EM fields in conductive media. At the frequencies of interest for geologic exploration, EM fields diffuse through conductive media rather than propagate as waves. An analogy is heat conduction through a metal plate. Consequently, it is difficult to resolve sharp boundaries in the absence of other information. Although models with more complicated structure and sharp boundaries may be consistent with the observed data, they are rarely required by the data, and this distinction is an important issue in determining what features are resolvable by the data.

3.2   Optimization Algorithms

EM tomography is a computationally intensive problem. The forward problem entails solving a large matrix system, and numerical optimization algorithms are needed to perform the minimization of the objective functional, Φ.

Our current tomography software includes two algorithms for minimization of the objective functional (Rodi and Mackie, 1999). One is the "successive linearized inversion" scheme described by Zhang et al (1995) and based on earlier work by Mackie and Madden (1993). This scheme, which can be categorized as a version of the Gauss-Newton method (Tarantola, 1987), solves a linearized inverse problem in an iterative loop until an acceptable value of Φ is achieved. We can then solve the linearized problem iteratively using a conjugate gradient (CG) technique. The CG technique requires the computation of linearized forward and adjoint operations; Zhang et al developed highly efficient algorithms to perform these operations, building on earlier work by Madden and Mackie (1989), Rodi (1976) and Mackie and Madden (1993). The EM forward problem is itself solved with another version of the CG method.

The other optimization algorithm we have implemented is a nonlinear conjugate gradient algorithm (Rodi and Mackie, 1999), an approach also used by Ellis and Oldenburg (1994). Unlike the Gauss-Newton method, nonlinear CG does not solve a linearized inverse problem at each step of an iteration. Instead, at each step it performs a line (one-parameter) minimization along a given direction in model space. The model direction at each step is derived from the gradient of the objective functional for the current model and the direction and gradient from the previous step. A pre-conditioning operator is applied to the gradient vector in an attempt to find the most important directions in model space in the early iterations. The same efficient algorithms for forward and adjoint operations, used in the other inversion scheme, may also be used in nonlinear CG.

Our experiments with the nonlinear CG method to date indicate that it is extremely fast if a good pre-conditioning operator is used. For example, inversions of real data with up to 120 stations and 20 frequencies per station were accomplished on a desktop workstation in less than an hour with the nonlinear CG scheme whereas the same inversion would not have been possible with standard matrix inversion Gauss-Newton algorithms. The nonlinear CG method has been tested on a wide variety of real and synthetic data and has been found to give exemplary results.

3.3 Parametric Inversions

Minimum structure inversions are useful because they yield models that contain only the minimal amount of structure in the subsurface required to fit the observed data, and they do not contain features that are incidental to the way in which the models were obtained. Additionally, it is

possible to test various geological hypotheses in the minimum structure framework by the inclusion of an *a priori* model. The inversion routine then finds the minimum variations away from the *a priori* model that are necessary to fit the data.

However, there may be situations where smooth gradational models are not optimal in terms of geological and geophysical interpretation. For example, there are many geological provinces where the subsurface geology is fairly simple and well known—it may consist of basically two or three distinctive units which are separated by sharp boundaries. Another example is the case of a tunnel in an otherwise fairly homogeneous background. Here, the tunnel, which is very resistive, is sharply distinct from the more conductive background. The problem, then, is to determine the geometry of those units in a particular location within that geological province. With minimum structure inversions, one would only be able to determine gradational representations of those boundaries rather than the boundaries themselves. While this may be consistent with the physics of EM diffusion in a conductive media, it is not ideal for the person who needs to know the geometry of these boundaries.

One way to deal with this is by use of parametric inversion algorithms (Portniaguine and Zhdanov, 1995). Instead of inverting for the smoothest model possible, one inverts for only a few parameters relating to simple geometrical bodies. For example, one could specify to invert for the parameters of a circular-shaped body in the subsurface that best fit the observed data. The inversion would then find the best-fitting location, radius, and conductivity contrast for this body. Although such structures would not necessarily be required by the data, as in a minimum structure inversion, it would allow one to test how well simple sub-surface geometries fit the observed data.

In our research, we have developed two parametric inversion algorithms: one algorithm that inverts for sharp boundaries with variable geometry, and another that simply inverts for a rectangle in a homogeneous background (the tunnel problem). In both algorithms, it is necessary to derive a scheme that projects discrete boundaries and resistivities onto the finite difference mesh used for the forward modeling. For the sharp boundary inversion, we assign discrete boundaries by specifying nodes with straight lines connecting the nodes. The resistivity of the layers are allowed to vary by assigning resistivity nodes within the layer and assuming the resistivity varies linearly between nodes. When interfaces cut across the blocks in the finite

difference mesh, we use a simple scheme that assigns the resistivity of that block as a weighted average of the resistivity above and below the interface. Sensitivities to changes in both the interface node locations and the resistivities of the layers can be computed efficiently by the calculus chain rule and use of the same efficient forward and adjoint operations involved in the minimum structure inversion scheme. For the tunnel inversion, we assume a homogeneous background and simply project the tunnel onto the finite difference mesh, again using a simple weighted average of resistivities where the tunnel boundary crosses blocks in the finite difference mesh.

3.4 Simple Example of Parametric versus Smooth Inversion

Synthetic MT data were generated for a simple two-layer model with a sloping ramp interface, but the details of the model were unknown until after imaging with the sharp boundary inversion algorithm (the model and synthetic data were kindly provided by a colleague). Random Gaussian noise at a level of 5% were added to the synthetic data and these data were then imaged by both the minimum structure algorithm (Figure 1) and the sharp boundary algorithm (Figure 2). It was later determined that the sharp boundary inversion came within a few percent of the correct location and geometry of the interface. It is clear from the figures that although the minimum structure inversion results in a model that has the correct overall features, it would be difficult from that result to locate boundaries between the conductive and resistive units. In this simple case, the sharp boundary inversion is superior to the smooth model result. We should stress again, however, that the sharp boundaries are not inherently resolvable from the data except when we specify *a priori* that the resulting model will have sharp boundaries.

An example using the second parametric inversion routine, to solve for a simple rectangular tunnel in a homogeneous background media, is illustrated in the next section.
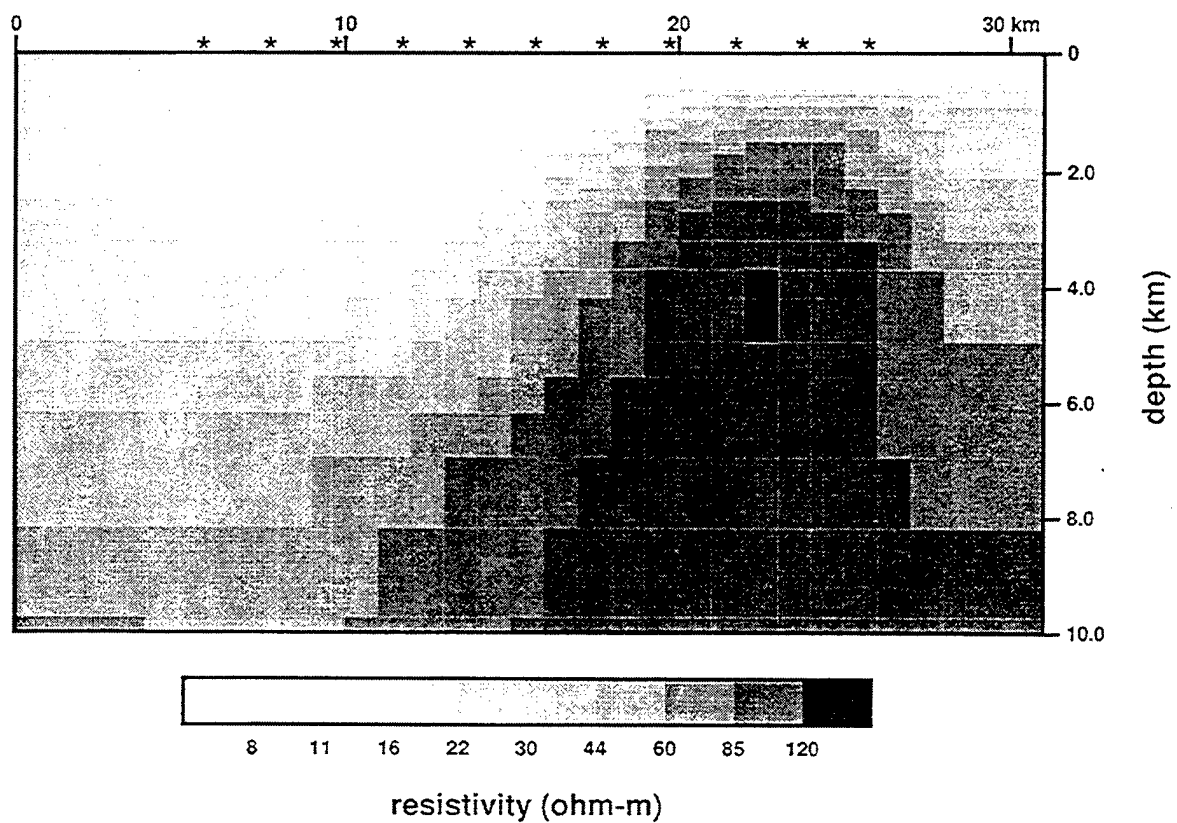
9

Figure 1. Smooth model inversion of synthetic ramp data.

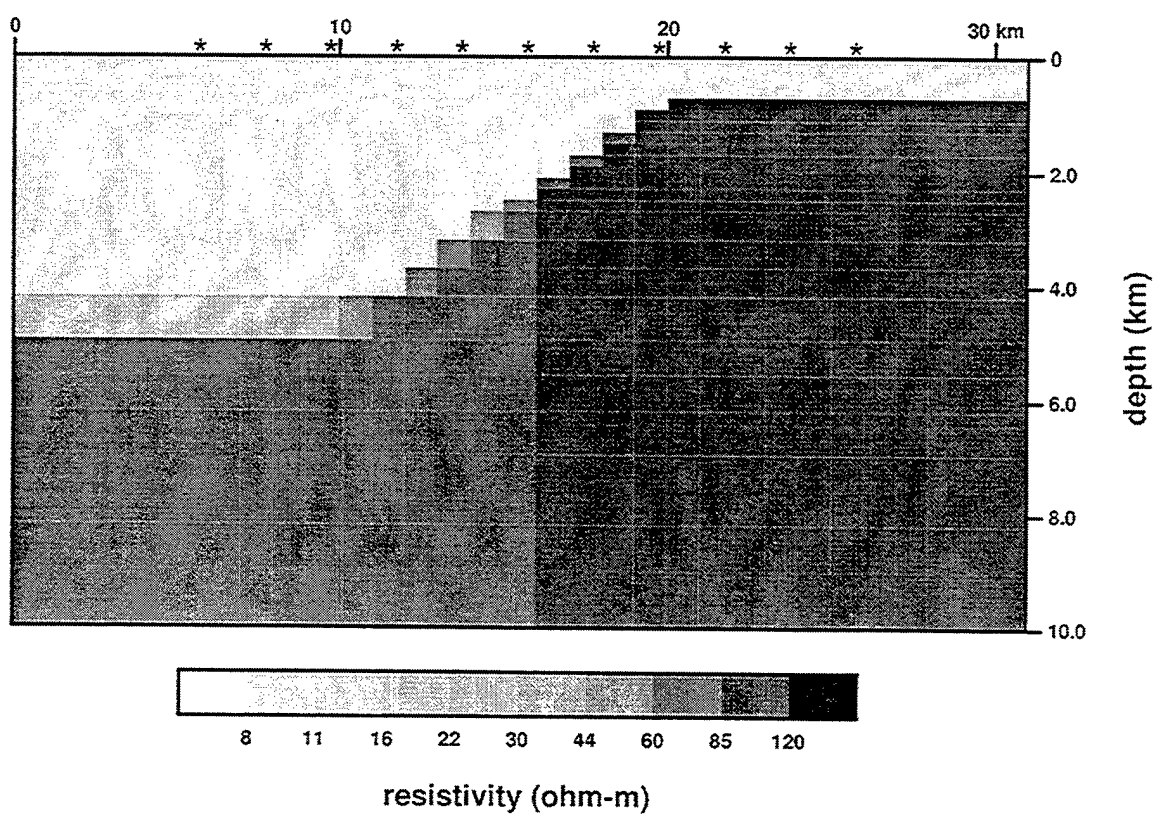# Sharp model inversion of Synthetic Ramp Data

TM mode

Figure 2. Sharp boundary inversion of synthetic ramp data.

4. Sensitivity of EM data to underground tunnels

4.1 Geometric and Resistivity Effects

Of primary importance in detecting underground tunnels is the sensitivity of surface EM data to the size and depth of underground structures. That is, tunnels that are too deep or too small will not have an observable surface signature and therefore will not be detectable regardless of the imaging algorithm used. Consequently, it is critical to the success of underground tunnel detection to determine the depths and dimensions at which underground tunnels have some reasonable chance of exhibiting a surface signature, above and beyond the normal background geologic signature.
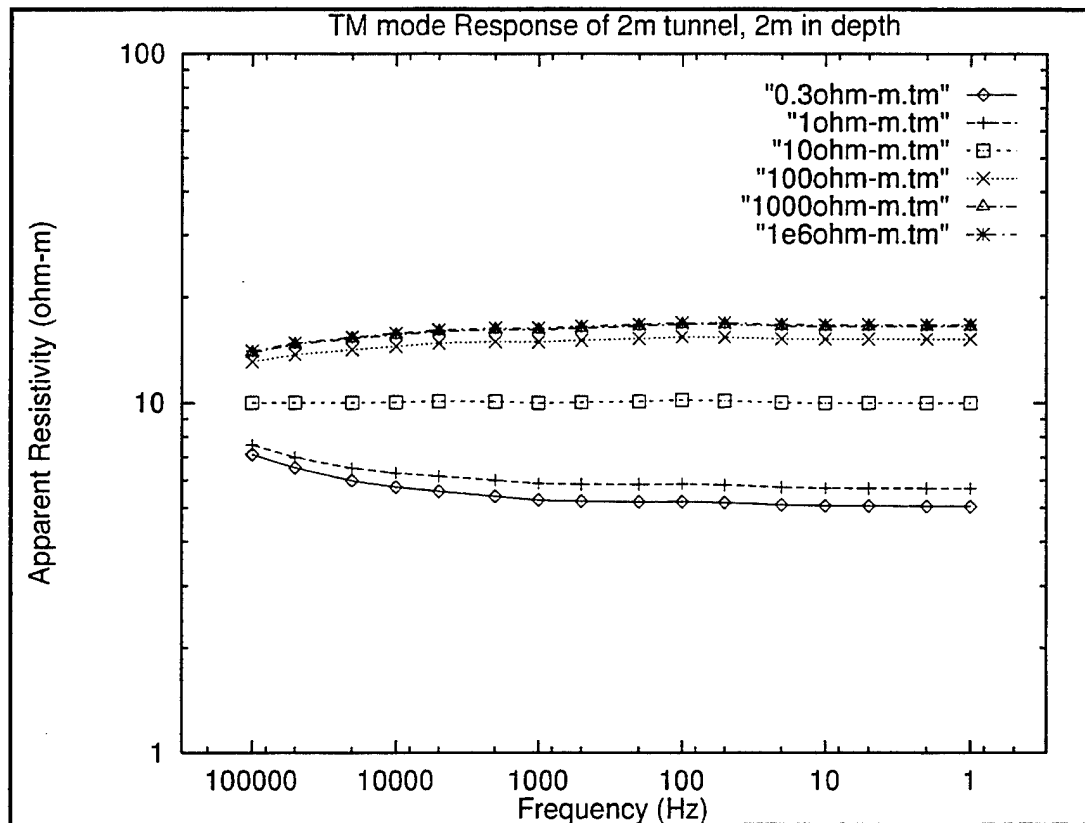

Figure 3. TM mode amplitude response of 2x2 meter tunnel at 2 meters depth. The apparent resistivity responses are shown for various resistivities of the tunnel.

Therefore, we have examined the sensitivity of EM data to subsurface tunnels by computing synthetic data for simple models, using finite-difference modeling algorithms. In particular, we have concentrated on models that attempt to simulate subsurface tunnels at different depths and sizes. The first model tested was a 2m by 2m square (of varying resistivity) buried in a homogeneous 10 ohm-m background media. This is perhaps the simplest model and represents an upper boundary for detection of subsurface tunnels (the real earth is not homogeneous and field measurements always are contaminated by noise). Figure 3 shows the TM mode apparent resistivity as a function of frequency and tunnel resistivity for this model when the top of the simulated tunnel is at a depth of 2 m. This result is for a station 0.125 m off the center of the simulated tunnel. Figure 4 shows the TM mode phase response for the same model and also for varying tunnel resistivities. Over most of the frequency range, the TM response appears as a static shift.
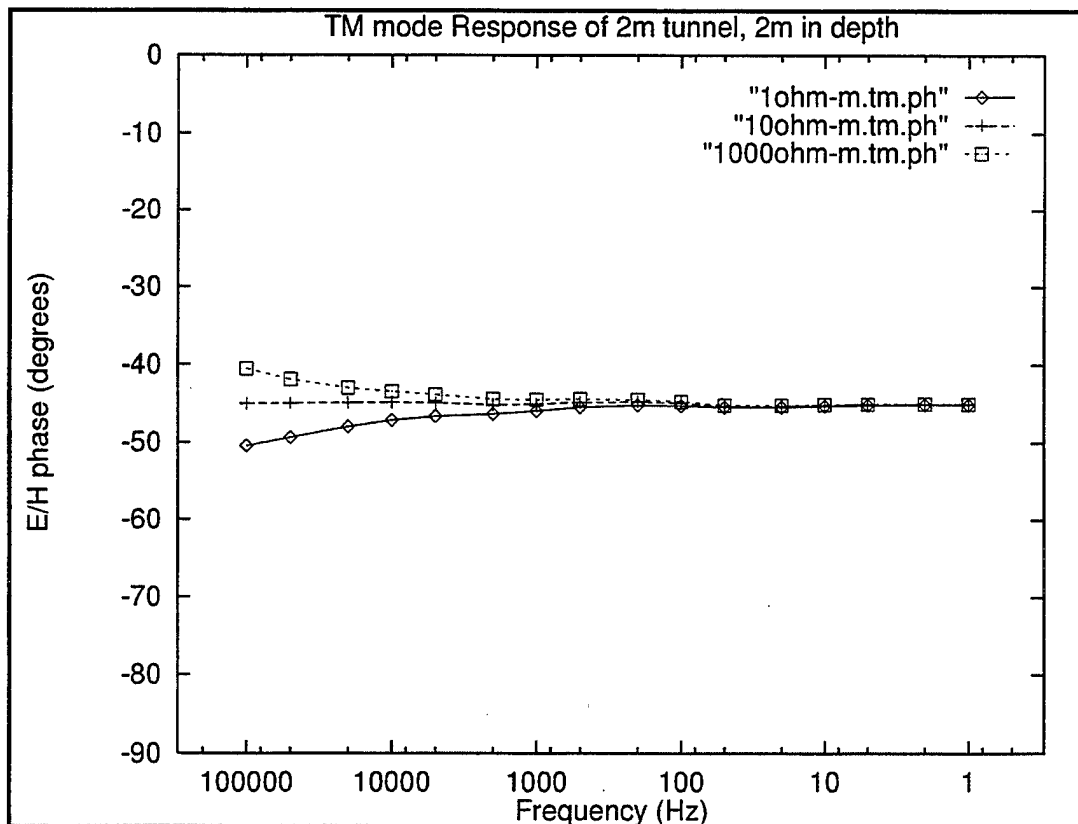

Figure 4. TM mode phase response of 2x2 meter tunnel at 2 meters depth. The phase responses are shown for various resistivities of the tunnel.

The TE mode apparent resistivity and phase for this same model are shown in Figures 5 and 6. These figures demonstrate a well-known aspect of MT, which is that TE mode data are sensitive to conductive bodies and have very little sensitivity to resistive bodies. This is due to the gathering of current into the infinite extent (in 2D models) of a conductive body, whereas the currents merely flow around a resistive body. From these figures one can deduce that a conductive body is more resolvable than a resistive body, and indeed this is borne out by inversions of these synthetic data. Figure 7 shows the minimum structure inversion result for the synthetic data where the subsurface body was 1 ohm-m, whereas Figure 8 shows the result where the body was 1000 ohm-m. The true model is a 2m by 2m square at a depth extent from 2 to 4m. Note the conductive body is well-resolved, because of the strong TE mode response, whereas the resistive body is less well-resolved, because it only has weak TM mode response and no TE mode response.
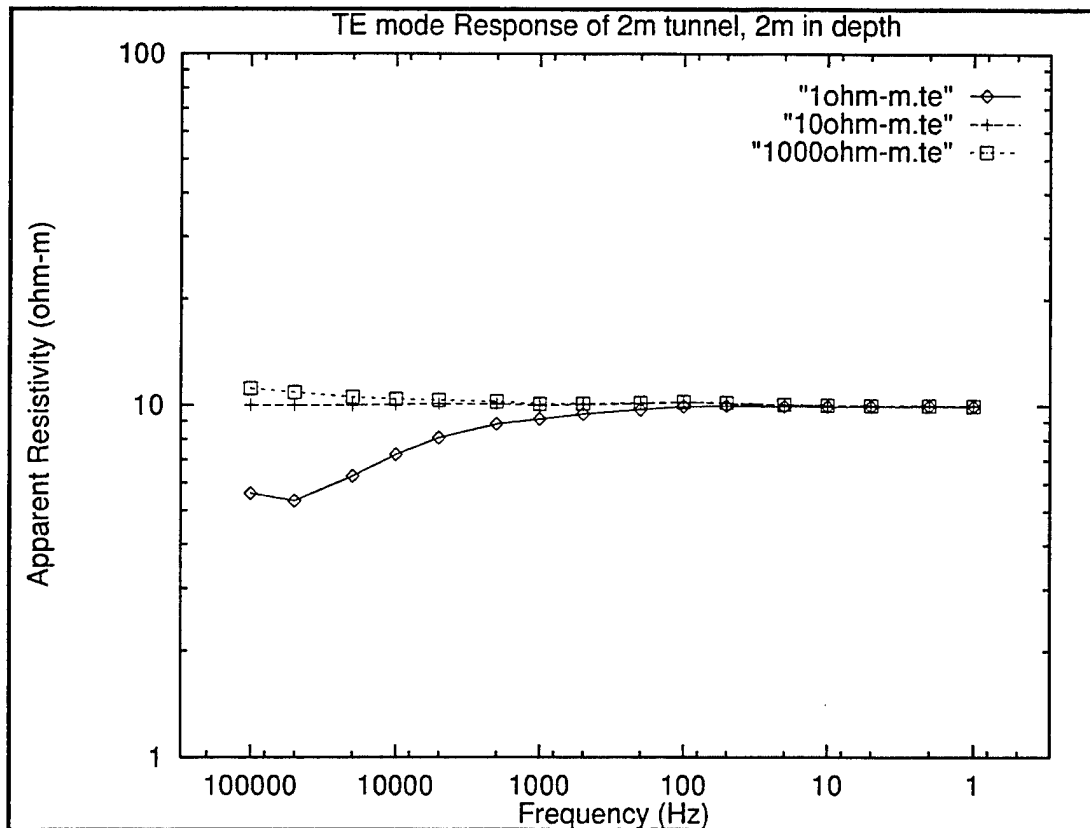

Figure 5. TE mode amplitude response of 2x2 meter tunnel at 2 meters depth. The apparent resistivity responses are shown for various resistivities of the tunnel.

This demonstrates that even under ideal conditions, tunnels, because they are likely to be resistive, will be difficult to detect.

The synthetic data shown in the previous examples were computed using our own finite difference modeling algorithms. To ensure against numerical inaccuracies, we have compared our finite difference responses to the responses computed for the same models using Phil Wannamaker's finite element code. The comparison is shown only for the cases of the 1000 ohm-m square and 1 ohm-m square in a 10 ohm-m background. The results, Figures 9 and 10, indicate excellent agreement between the two modeling algorithms, with less than 0.5% differences.
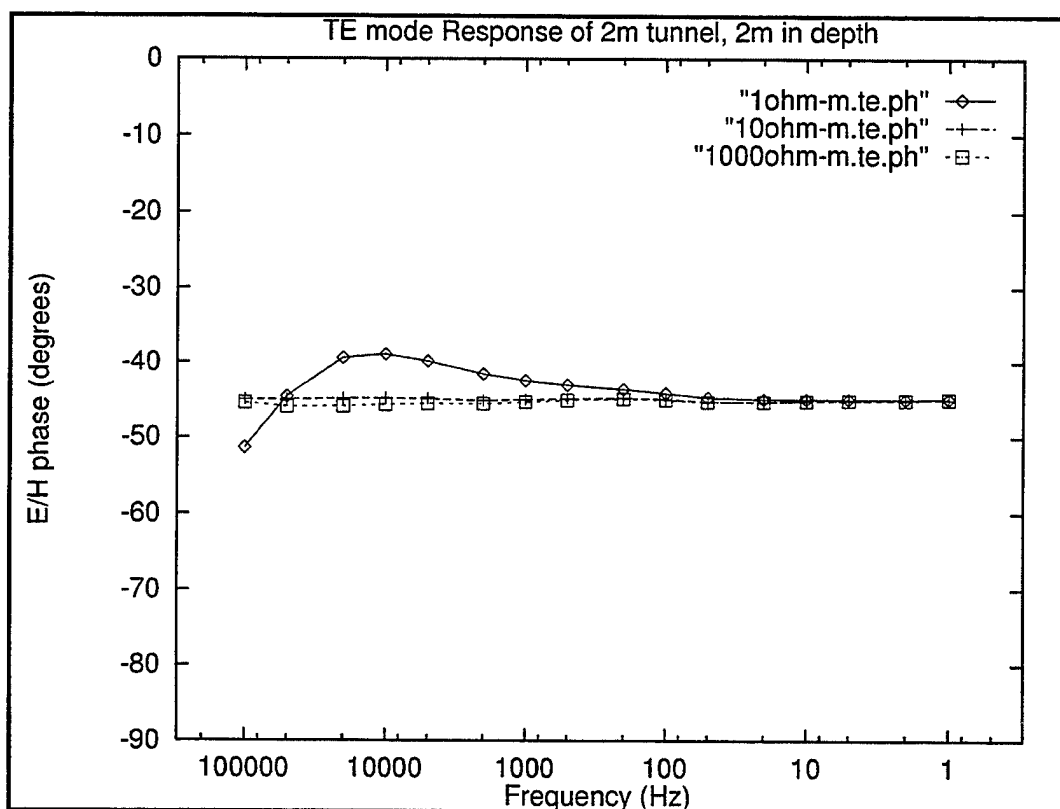

Figure 6. TE mode phase response of 2x2 meter tunnel at 2 meters depth. The phase responses are shown for various resistivities of the tunnel.

Conductive model inversion results
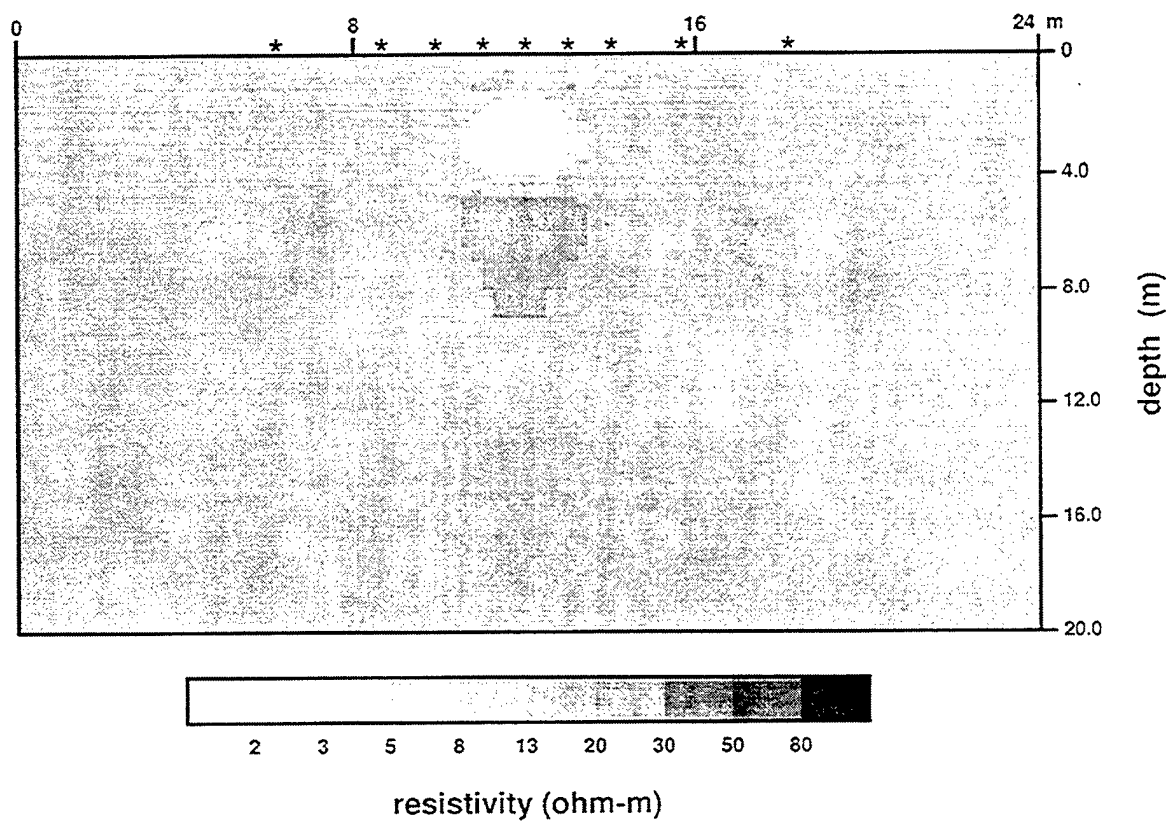
TM and TE mode

Figure 7. The minimum structure inversion of synthetic data over a conductive (1 ohm-m) 2x2 meter tunnel at a depth of 2 meters in a background media of 10 ohm-m. Note the body is well resolved.

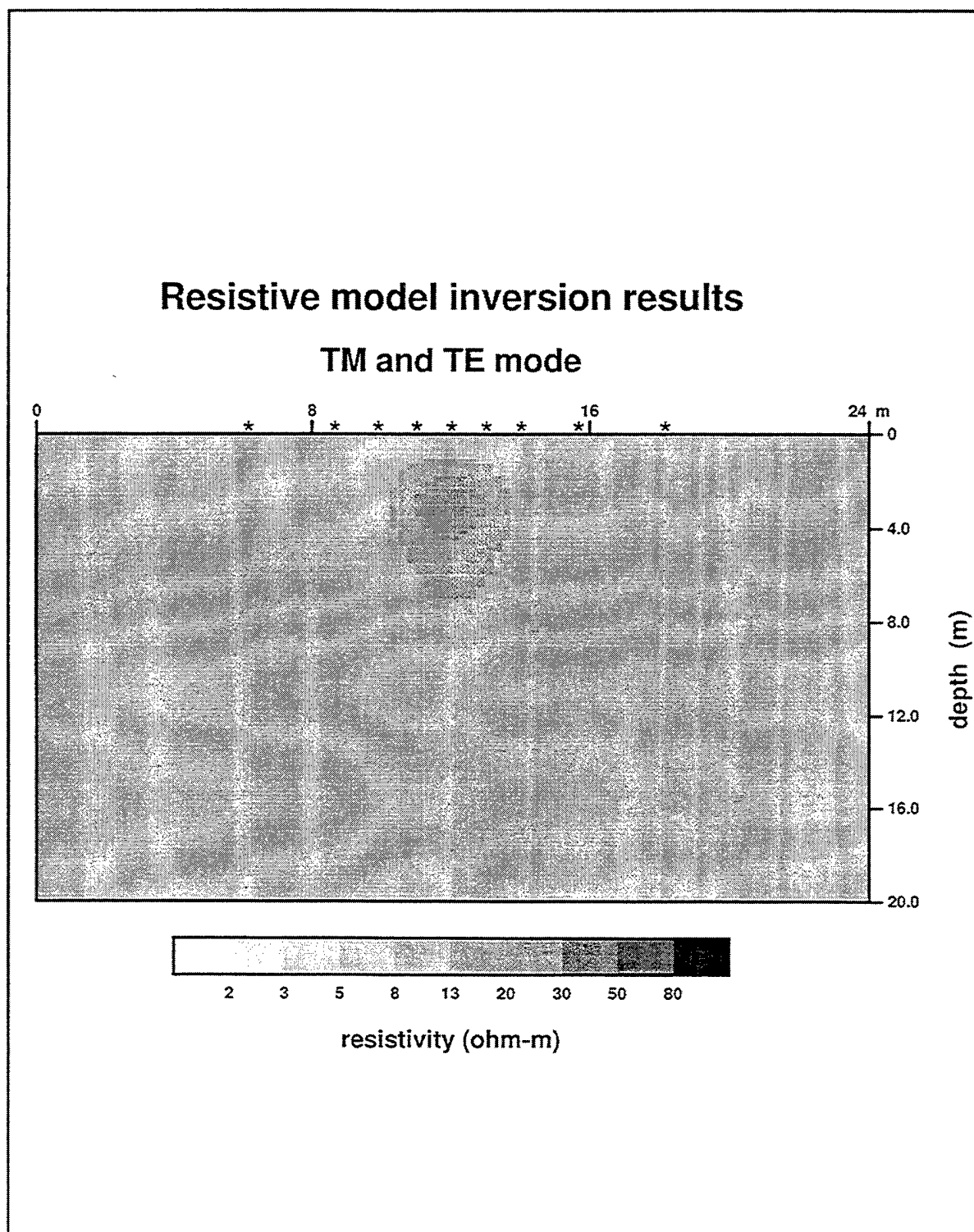# Resistive model inversion results

TM and TE mode

Figure 8. The minimum structure inversion of synthetic data over a resistive (1000 ohm-m) 2x2 meter tunnel at a depth of 2 meters in a background media of 10 ohm-m.
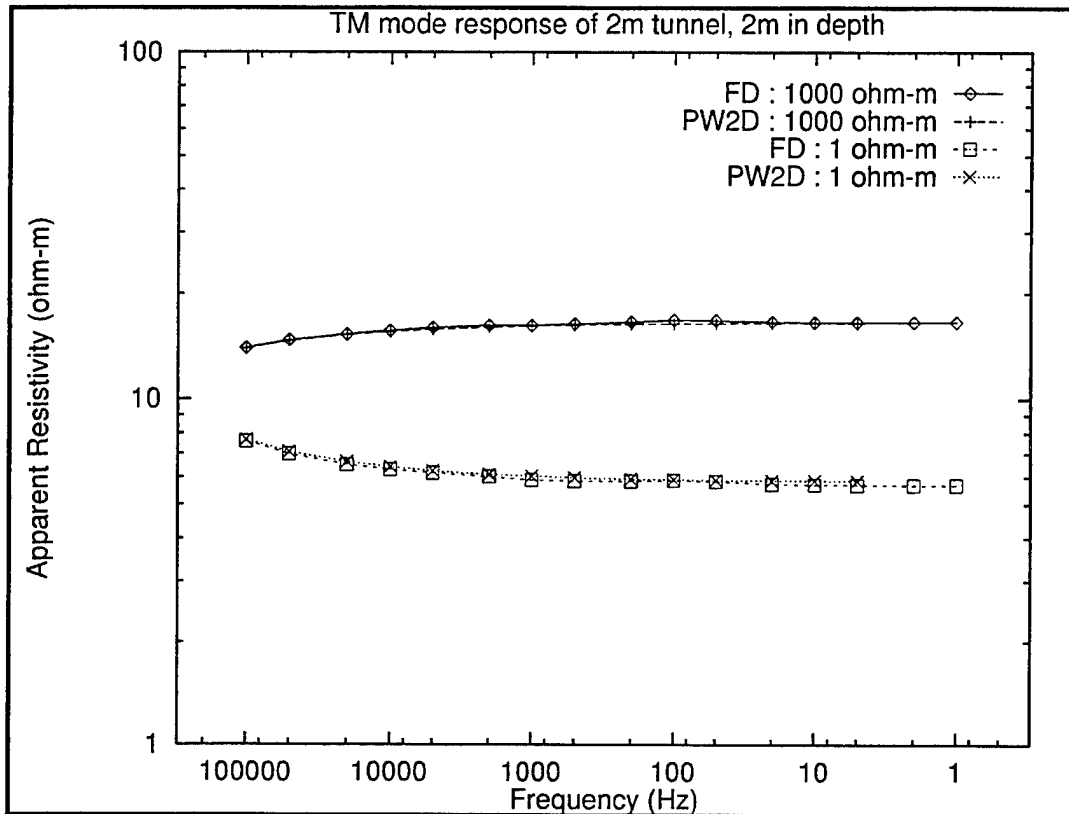
17

Figure 9. TM mode amplitude response comparing our finite difference algorithm and Phil Wannamaker's finite element algorithm.
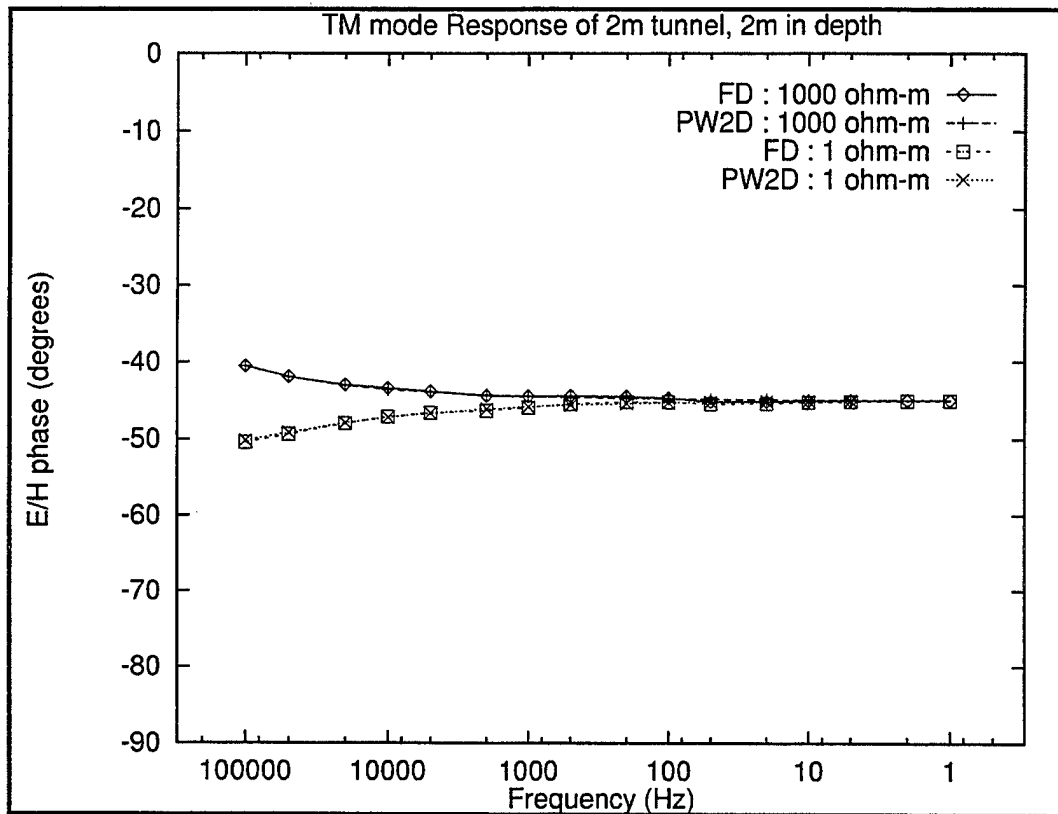
Figure 10. TM mode phase response comparing our finite difference algorithm and Phil Wannamaker's finite element algorithm.

Next, we varied the depth to the top of the 2m by 2m simulated tunnel, and in each case, computed the synthetic responses for varying resistivities of the tunnel. The TM mode apparent resistivity is shown for the cases when the depth to the top of the tunnel is 4m (Figure 11) and 6m (Figure 12). The TE mode apparent resistivity for the case when the depth to the top of the tunnel is 6m is shown in Figure 13. It is clear from these figures that by the time the subsurface body is at a depth/diameter ratio of approximately 3-4, the response is extremely weak and would be very difficult to detect under normal field conditions. The other important point from these simulations is that the frequencies that are sensitive to observable subsurface tunnels are typically above 1000 Hz, a range where it is sometimes extremely difficult to get good data because of the AMT dead band, an issue that will be discussed shortly.

19

Figure 11. The TM mode amplitude response of a 2x2 meter tunnel at 4 meters depth. The apparent resistivities are shown for different tunnel resistivities.

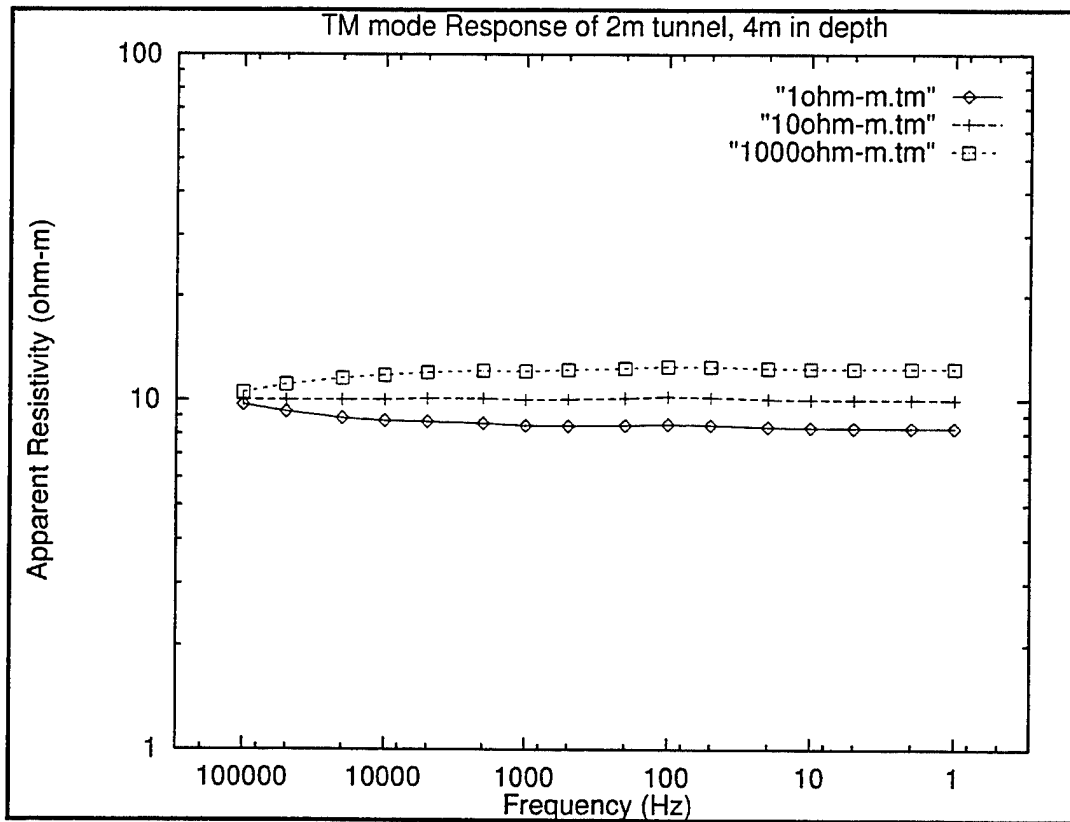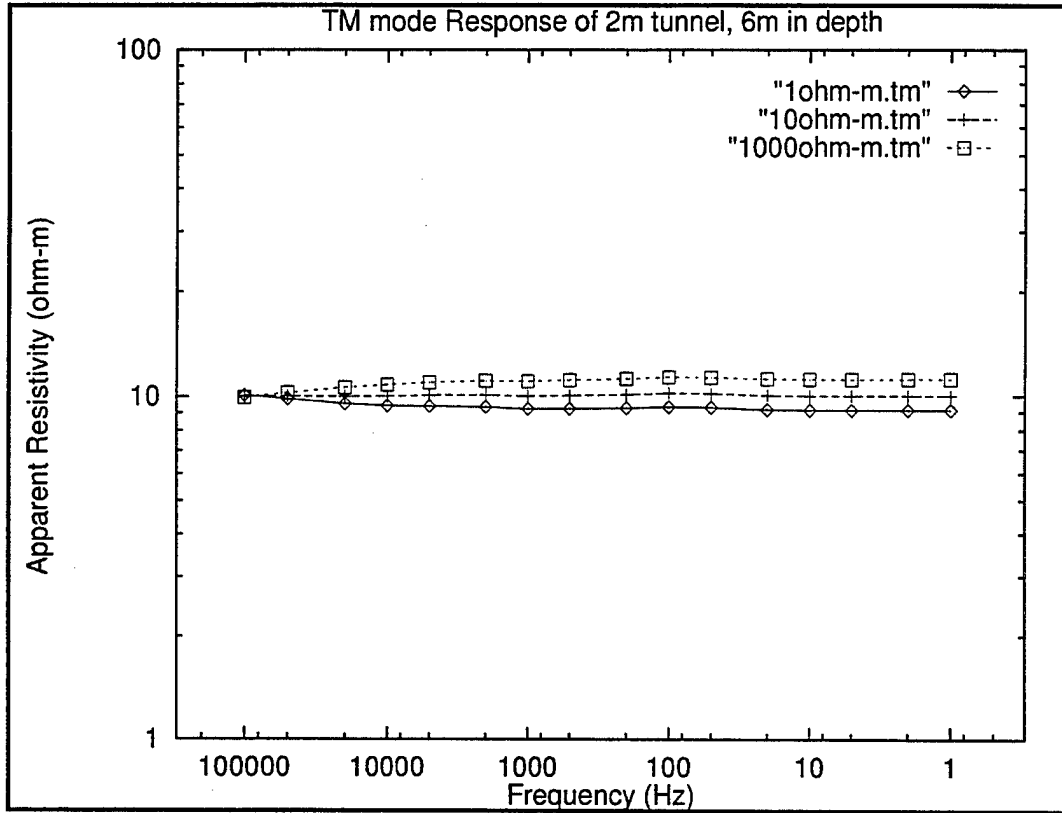**Figure 12. The TM mode amplitude response of a 2x2 meter tunnel at 6 meters depth. The apparent resistivities are shown for different tunnel resistivities.**
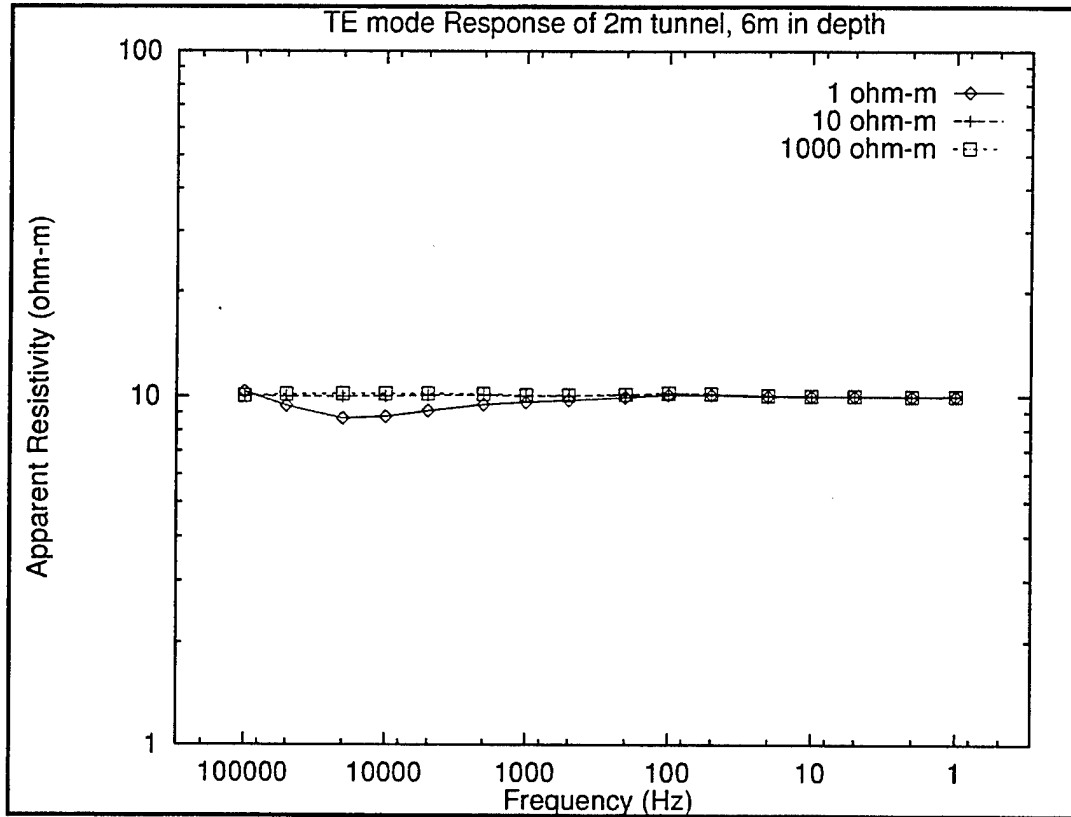
Figure 13. The TE mode amplitude response of a 2x2 meter tunnel at 6 meters depth. The apparent resistivities are shown for different tunnel resistivities.

The previous examples showed the results of using minimum structure inversion algorithms to invert the synthetic data from simple models simulating shallow tunnels. For the case where the tunnel had a depth/diameter ratio of 1, the minimum structure algorithms were able to resolve both conductive and resistive bodies quite accurately. We then applied our parametric inversion algorithms to these same data, solving for the best location of a rectangular body as well as the resistivity of the body and the background. The model resulting from a parametric inversion of synthetic data for the conductive body is shown in Figure 14, and the model resulting from a parametric inversion of synthetic data for the resistive body is shown in Figure 15. In both cases, the results from the parametric inversion match nearly perfectly the parameters for the true synthetic model (2mx2m with the top of the tunnel at 2m depth).
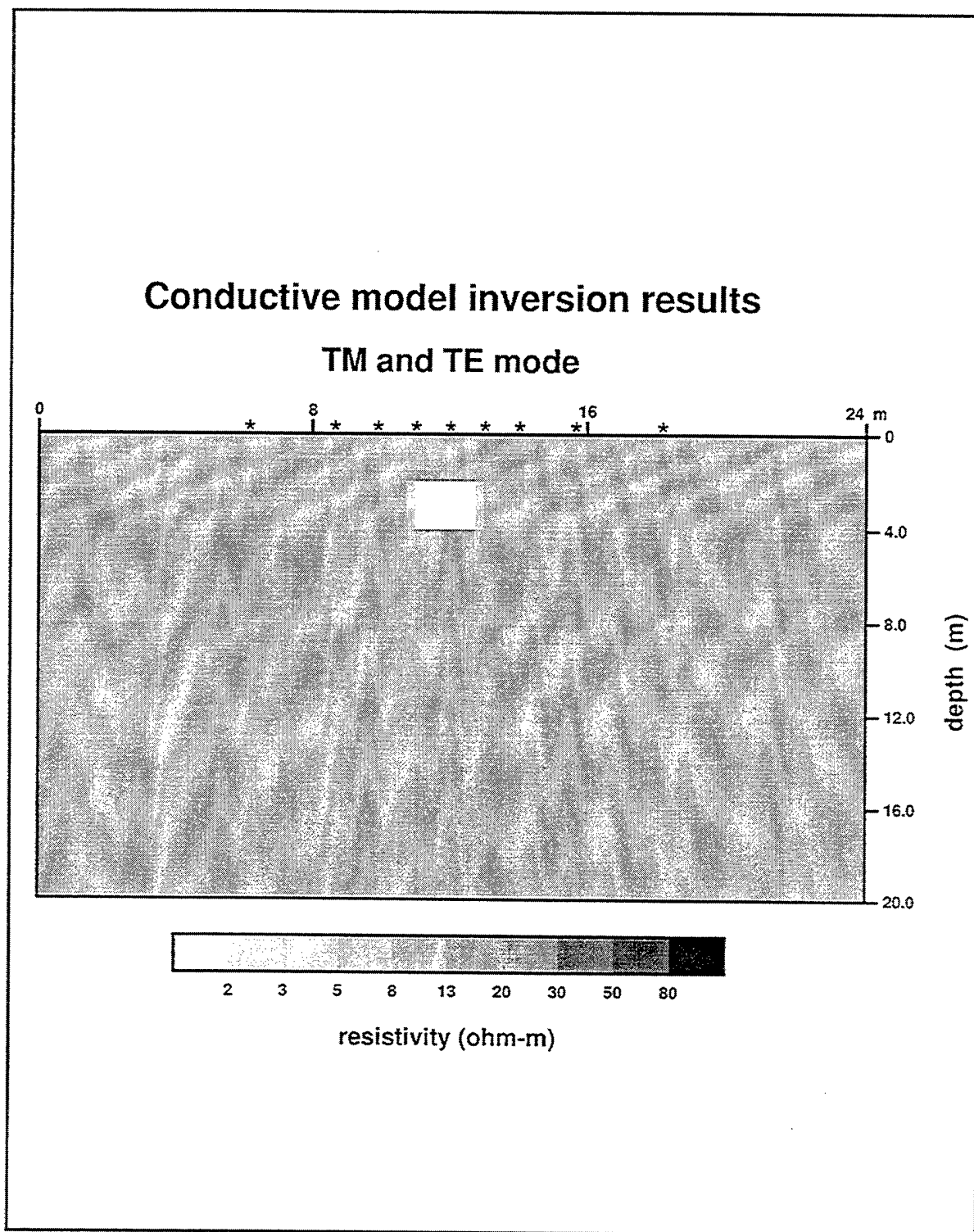
Conductive model inversion results

TM and TE mode

Figure 14. Parametric inversion for a conductive tunnel of dimensions 2x2 meters at 2 meters depth.

Resistive model inversion results
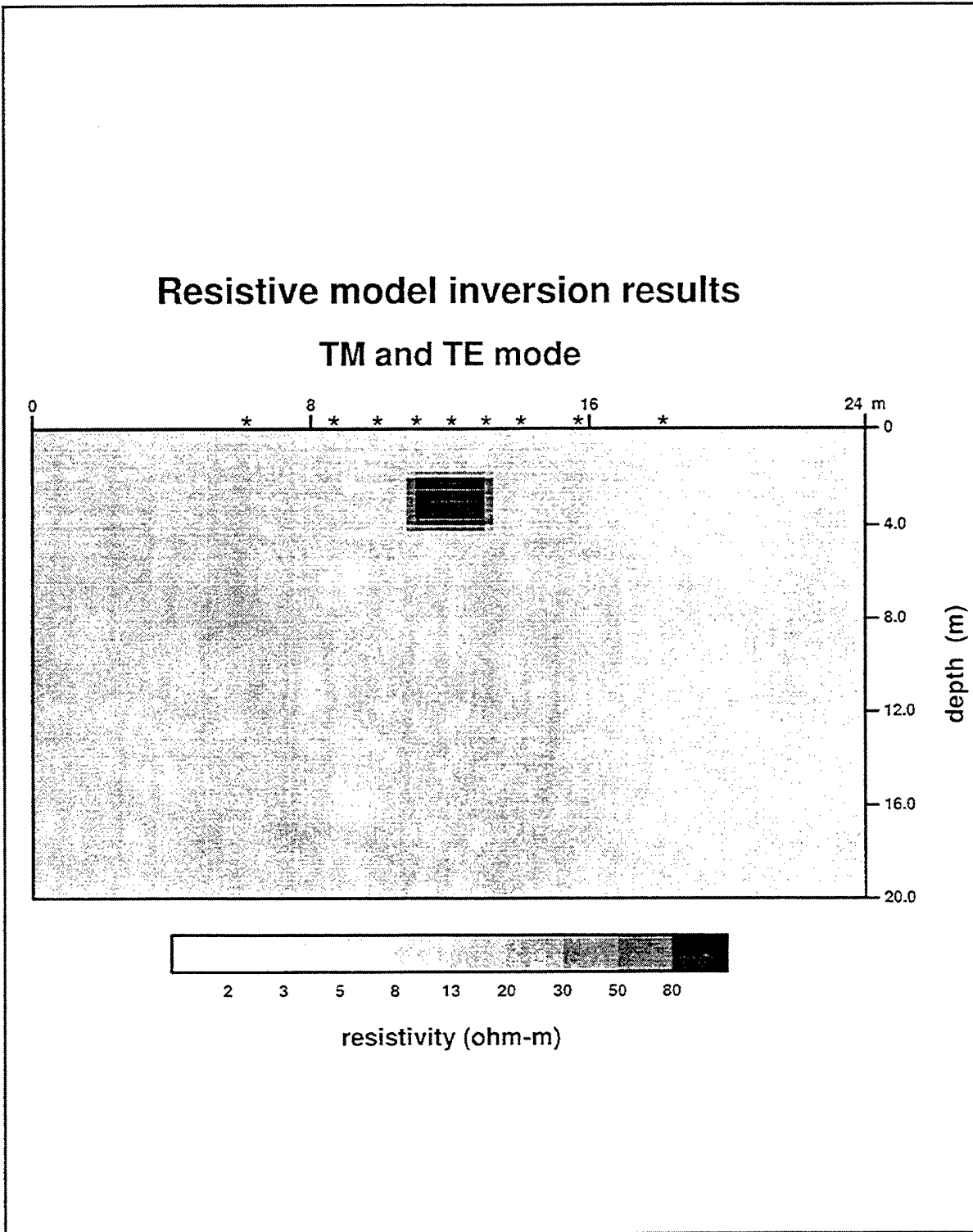
TM and TE mode

Figure 15. Parametric inversion for a resistive tunnel of dimensions 2x2 meters at 2 meters depth.

4.2 The AMT Dead Band

Natural electromagnetic fields arise from a variety of sources. At low frequencies, the fields arise mainly from the interaction of earth's magnetic field with the solar wind. At frequencies between 10 and 500 Hz, the fields are due primarily to lightning strikes that produce EM waves that travel around in the earth-ionosphere waveguide. In this spectrum of natural fields, there are two well known dead bands (1 to 0.1 Hz, and 1000 to 2000 Hz), that arise from a lack of signal and from attenuation in the earth-ionosphere cavity. The most severe of these dead bands is the AMT dead band in the 1000 to 2000 Hz range. This dead band is important for tunnel detection because it is right in the range that is usually critical for detecting subsurface tunnels. We have carried out independent research on this topic and found that even using 24 bit digitizing systems, in general the magnetic field spectrum in the AMT dead band is *below* the inherent system noise of commercial coil magnetometers. Additionally, we have found that the natural fields in this band tend to be of greatest magnitude during the night hours. What this means in practice is that magnetic field measurements in this frequency band are very difficult to make reliably and hence, great care must be taken to ensure accurate measurements. This difficulty is obvious in some of the data analyzed later in this report. Electric field data do not suffer this same problem, because the electric fields can now be measured, using 24 bit systems, without any preliminary electronics or filtering. The main impact of these findings is that a reliable source would be extremely useful for collecting AMT data for tunnel detection.

5. Analysis of Data

In this section, we analyze four sets of MT data that were collected over known tunnel structures. The first three data sets were collected by Doug Klein from the USGS and were provided in order to test competing inversion algorithms for accuracy and robustness. The fourth data set was collected by APTI over the Silver Fox mine in Alaska.

5.1 San Xavier Data

The data in this experiment were collected along a profile oriented 338 degrees relative to true north. Electric and magnetic data were collected every 10 meters along this profile. An EMI 'TX-IM1' transmitter located approximately 300 m southwest of the line was used as a controlled

inductive source. The purpose for using a controlled source in geophysical surveys is to obtain data with high signal/noise ratios, especially in environments where natural MT signals may be difficult to collect because of local electrical noise sources.

The supplied data files from the blind test were input into a WinGlink[1] data base for further analysis and consisted of both controlled-source data, and some natural field MT data that were collected at only a few of the sites. A visual assessment of the data indicated generally poor data quality with a wide scatter between frequencies. An example of a typical sounding is presented in Figure 16, which shows the sounding curves from site BA17.
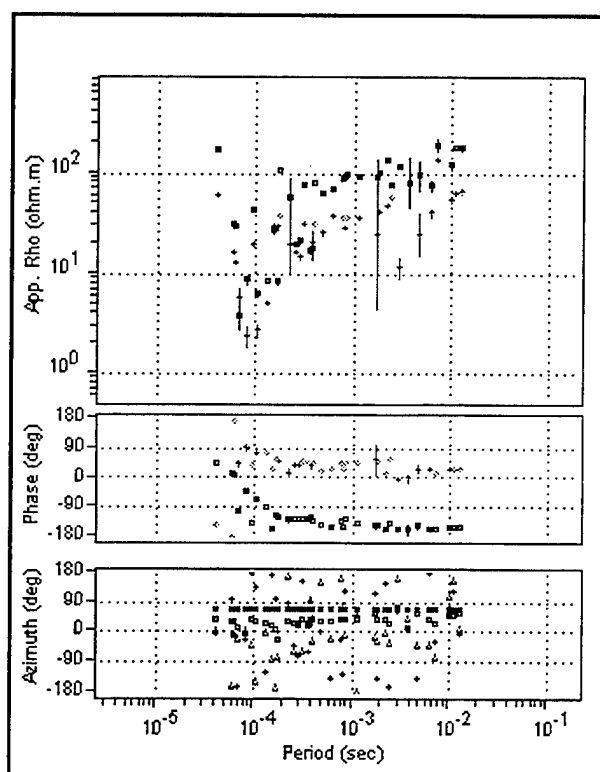
Figure 16. An example of a typical sounding curve, site BA17.

Before interpretation, the data were manually edited on a site-by-site basis, first eliminating obvious outliers, then using the D+ algorithm (which computes the most consistent apparent

---

[1] WinGlink is a data base and interpretation program for magnetotelluric and other geophysical methods commonly used in geophysical exploration, and was developed by Geosystem, srl.

resistivity and phase curves for a given set of data) to help eliminate inconsistent data points. While this is a partially subjective exercise, it does result in data that are less noisy.

After editing the data from each site, the data were rotated into alignment with the profile direction and then output for inversion using our minimum structure inversion algorithm. We started the inversions from a uniform halfspace of 30 ohm-m. A minimum structure inversion of these data is shown in Figure 17. We must stress that since the data are of generally poor quality and only marginally useful, conclusions based on the results of the inversion should therefore be taken with appropriate caution. The tunnel under this line is located at approximately site BA10. The inversion puts in a conductive feature at this location, which according to Doug Klein is due to fluid-filled fractures. We would normally expect a tunnel to exhibit a resistive signature rather than a conductive signature. However, it is possible that the inversions are inaccurate because of the poor data quality.
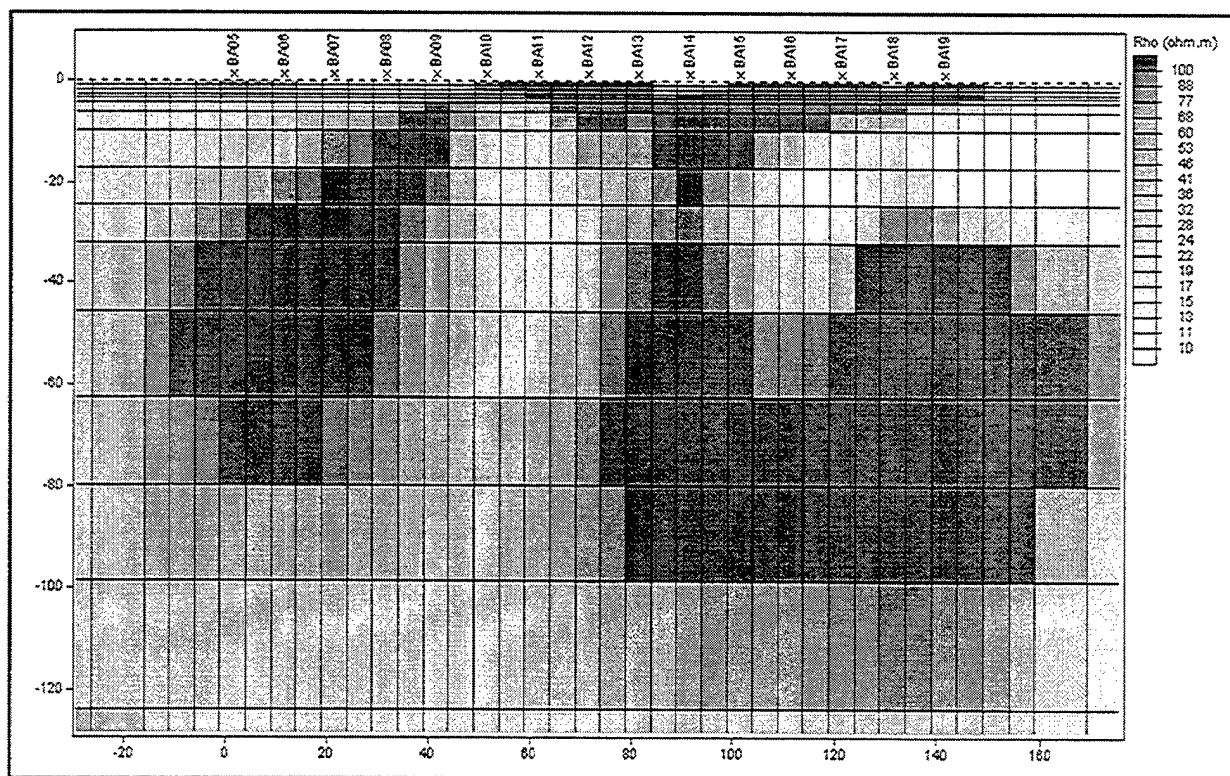

Figure 17. Minimum structure inversion of San Xavier MT data.

5.2 SSC tunnel

The data for this experiment were collected at the SSC tunnel in Waxahachie, Texas by Doug Klein of the U.S. Geological Survey. AMT data were collected at 15 stations spaced approximately 10 meters apart along a profile line perpendicular to the tunnel. The tunnel itself is believed to have been approximately 5 meters in diameter at a depth of 50 meters, giving a depth/diameter ratio of 10. The AMT data were collected using the MT-1 system manufactured by EMI. Natural source AMT data were collected at each site; additionally, lower frequency MT data were collected at a few of the sites, and controlled-source data were collected at 3 sites. Overall data quality is poor, similar to that observed in the previous data set.

All acquisition runs at each site were combined into one site response, converted to an EDI file, and then input into a WinGlink data base. The responses at each site were rotated to the strike direction of 162 degrees magnetic, and the TM (transverse magnetic) and TE (transverse electric) modes were output for inversion. Inversions were carried out starting from a uniform 10 ohm-m halfspace. Several inversions were run, but the main features were consistent among the various runs. An example of one such run is shown in Figure 18. A resistive feature is imaged, but at a depth shallower than the expected tunnel. This is likely an artifact of the poor data quality.
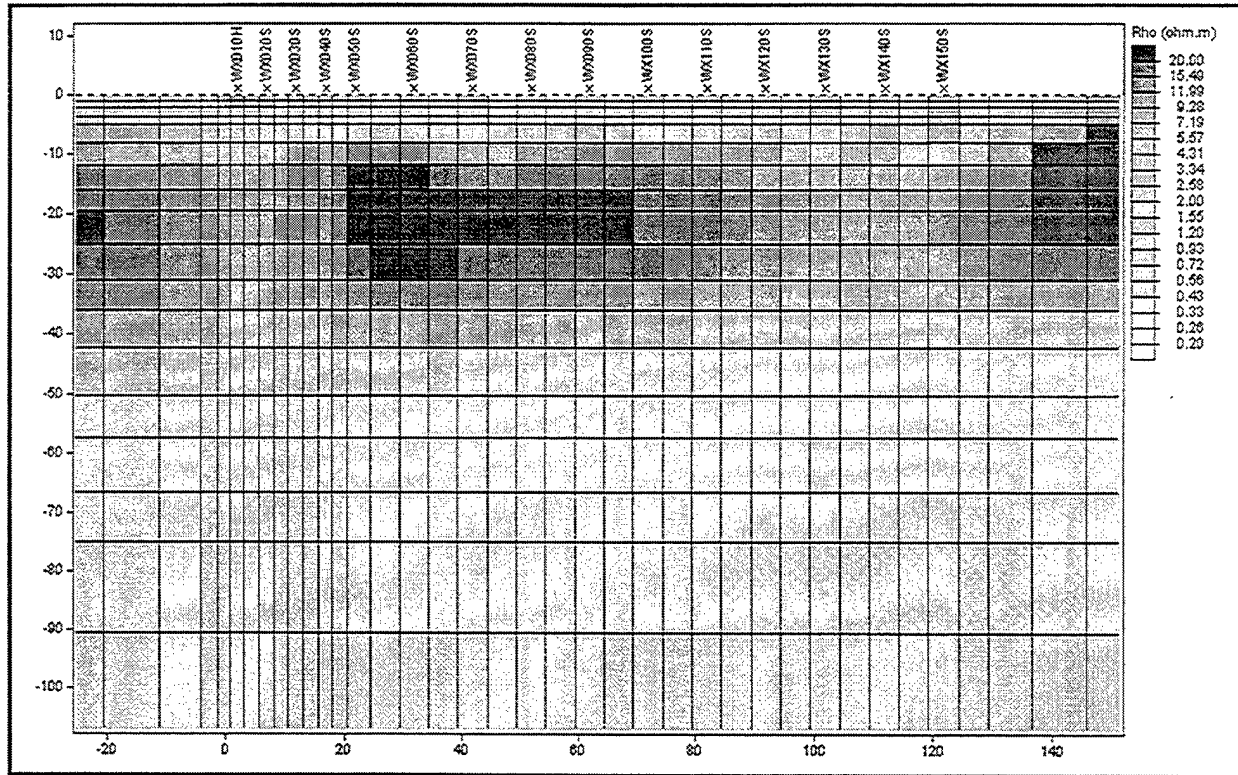
Figure 18. Minimum structure inversion of SSC data.

5.3 USGS Blind Experiment #2

The data from the USGS blind experiment #2, supplied by Doug Klein of the USGS, were supplied as impedance values, and these were converted to apparent resistivity and phases and then used for generating smooth 2D models. The data were synthetic data, generated for a model with 3 tunnels at depth to diameter ratios of 3:1, 10:1, and greater. We first inverted the noise-free synthetic data using our minimum structure inversion algorithm, with the results shown in Figure 19. There is an indication of a shallow resistive feature located near the 4th station (just to the right of the 50m mark on the Figure) and at a depth of around 15-20 m., which is likely the shallow tunnel. The tunnels located at greater depths appear not to be resolvable from this data set.

Inversion of USGS Blind Dataset 2
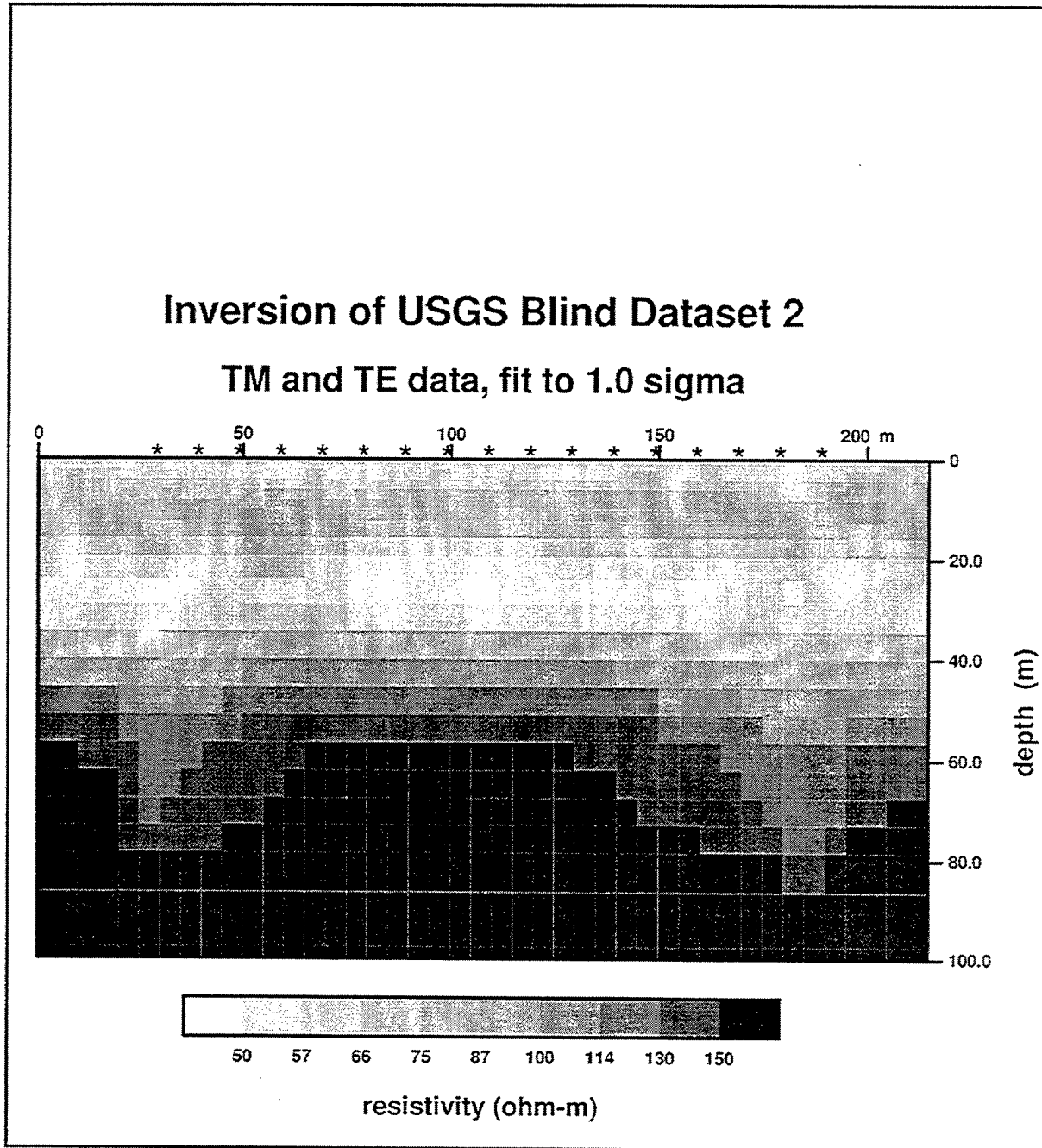
TM and TE data, fit to 1.0 sigma

Figure 19. Minimum structure inversion of noise-free USGS data from Blind Experiment #2.

To simulate geologic noise, we then added 5% random Gaussian noise to the synthetic data, and then imaged the data. The result, shown in Figure 20, is similar to the previous result in that only 1 tunnel is identified, but is probably more realistic than inverting noise-free data.

Inversion of USGS Blind Dataset 2
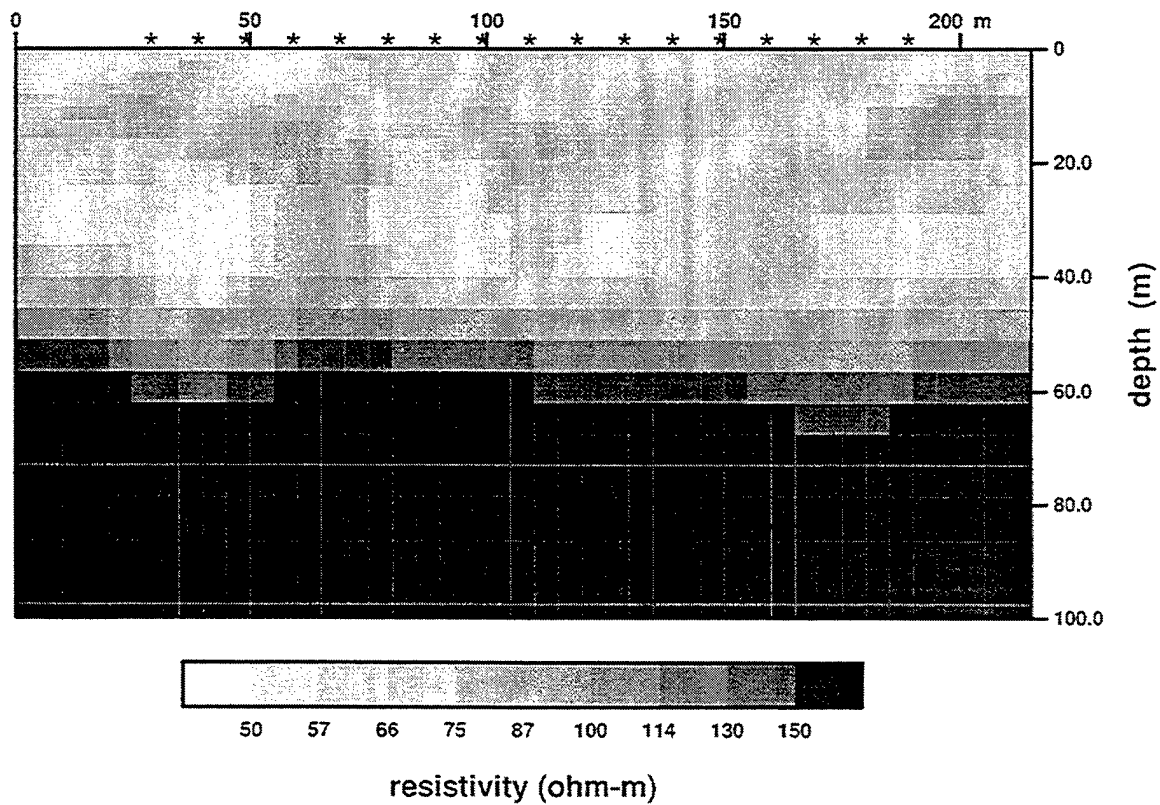
TM and TE data, fit to 1.2 sigma

Figure 20. Minimum structure inversion of USGS data with 5% random noise added.

5.4 Silver Fox Mine

The data from this experiment were collected by APTI during their 1995 Silver Fox Mine campaign using the HIPAS ionospheric heater some 40 km away from the experiment site. This transmitter is similar to that being constructed in the HAARP facility. We first analyzed the amplitude spectra from several sites and for different frequencies of transmitted signal. Figure 21 shows the amplitude spectra at site 4 for a transmitter frequency of 995 Hz. While the spectra have clearly defined spectral lines (peaks in the spectra), these lines are consistent from site to site and for the different transmitter frequencies. Hence, these spectral lines must be related to background signals (natural and artificial) and not to the signals being transmitted by the HIPAS source. In fact, it was difficult to find evidence of the HIPAS transmitted signals except at a few sites. Acting on a suggestion by APTI, we looked closely at site 5, and for a transmitted frequency of 2500 Hz we were able to identify spectral lines associated with the transmitted signal. The odd harmonics of this signal were especially strong.
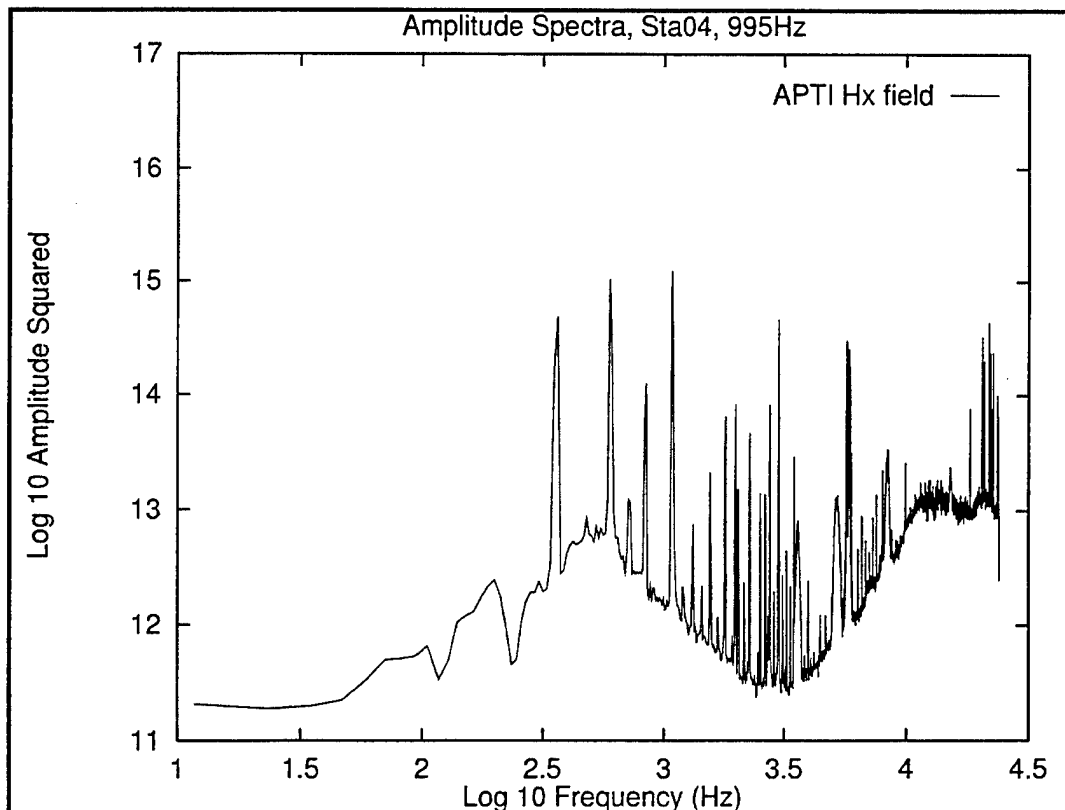

Figure 21. The amplitude spectra for site 04 at a transmitter frequency of 995 Hz.

Since the transmitted signals were in general too weak to even identify, we simply proceeded to process the time series using the robust processing algorithms developed in conjunction with Dr. Jim Larsen of NOAA (Larsen et al., 1996). At all sites and for all transmitted frequencies, we found that the TM mode data (electric field perpendicular to the tunnel) were noisy and had low coherencies. The TE mode data (electric field parallel to the tunnel), however, were of much better quality. Unfortunately, it is the TM mode data that would be most sensitive to a resistive sub-surface tunnel. An example of the results of the robust processing is shown in Figure 22 for station 15. In this figure, the E1 direction is parallel to the tunnel (TE mode), and the E2 direction is perpendicular to the tunnel (TM mode).

The robust processed data were then used in a minimum-structure inversion. Both TM and TE mode data were included, but the TM mode data were assigned larger variances to reflect their lower coherencies. The result of the inversion is shown in Figure 23 as a color-shaded cross-section of the subsurface resistivity. An area of increased resistivity is indicated in this figure, with its peak located around the 4th station from the left, and at around 20 meters in depth, which is close to the actual location of the subsurface tunnel. It should be noted that the ability to detect and image this tunnel is not related to the transmitted HIPAS signals, which were mostly too weak to be recorded, but rather simply to the natural background AMT signals. If, however, the transmitted HIPAS signals were stronger, they could play a valuable role in imaging the Silver Fox Mine tunnel.
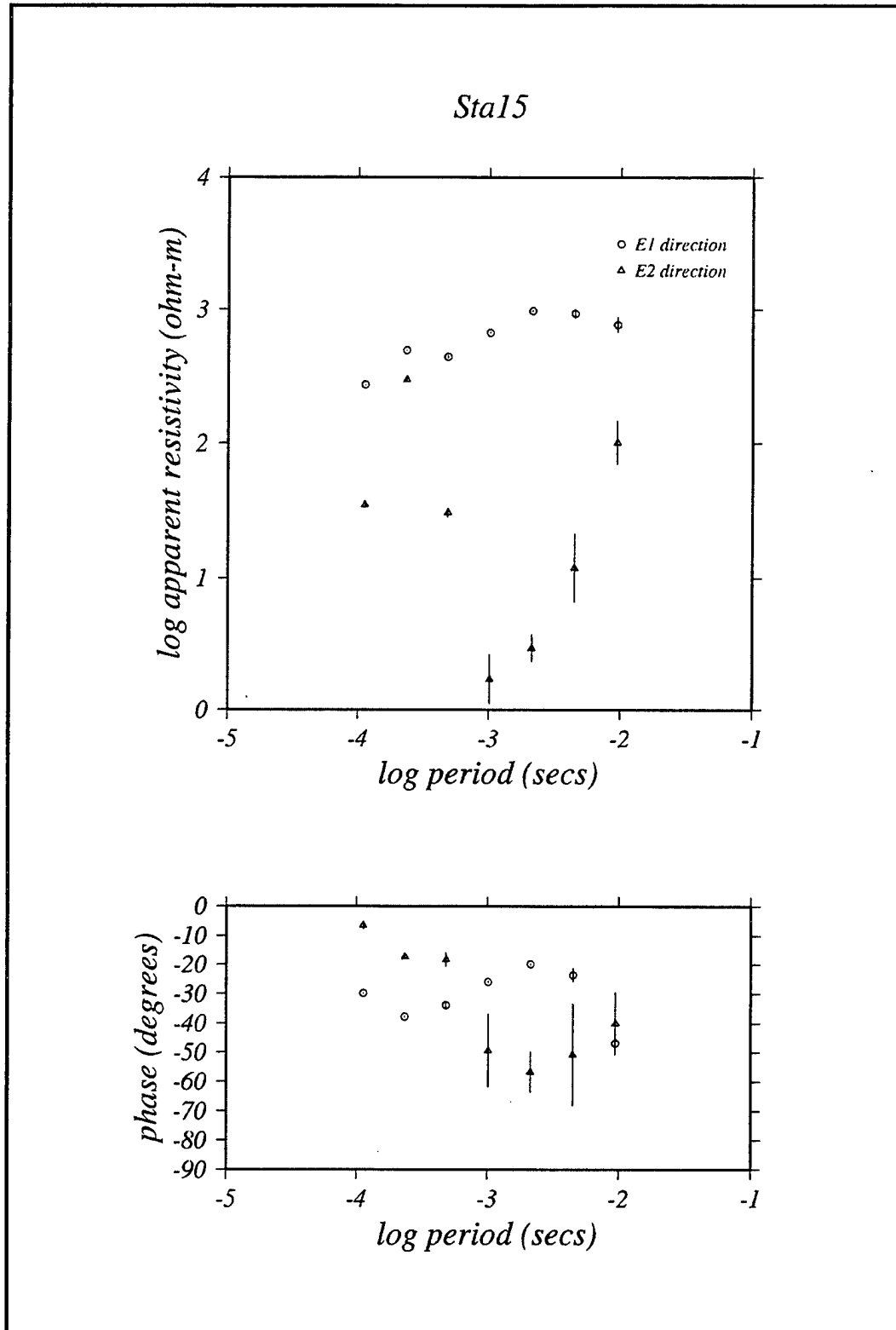
Figure 22. An example of robust processing applied to the data from station 15. The E1 direction is parallel to the tunnel, and the E2 direction is perpendicular to the tunnel.

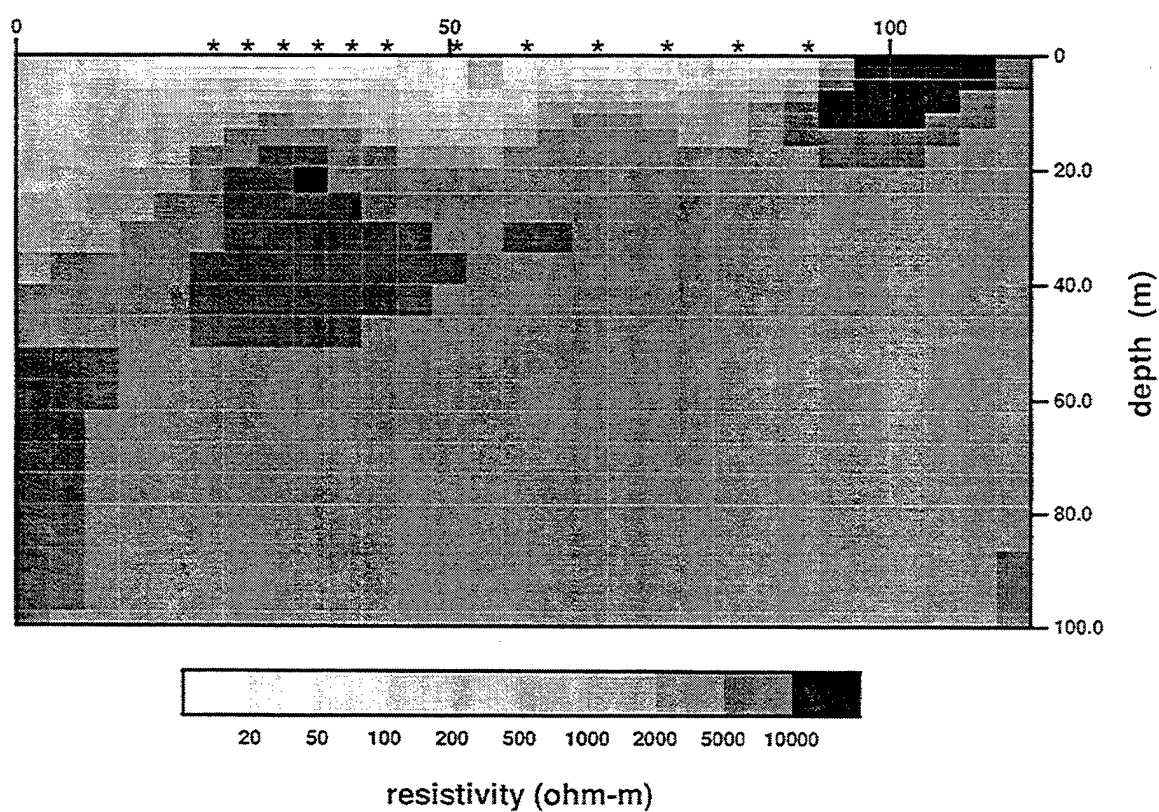# Inversion of APTI Silver Fox Dataset

TM and TE data

Figure 23. Minimum structure inversion result of Silver Fox Mine data.

6. Robust Processing Algorithm

AMT data present special problems, compared with MT data, due to local lightning sources, low signal levels around 1-2 kHz, changes in the transmitter frequency between data sections and single site data limiting the analysis to least squares biased by magnetic noise.

The robust processing code used to obtain transfer functions was originally developed for MT data (Larsen et al., 1996). It was recently modified by Dr. Larsen to allow for the changing frequency of the transmitter by developing a data selection process for each frequency band. Local lightning effects were excluded by examining the time domain residuals. It was necessary to set the outlier detection threshold higher than for MT data so that only the really local lightning were excluded. An example of this is shown in time series collected in an AMT experiment over a tunnel near Ridgecrest, California. In this example, there is also a local induction transmitter located some 200 meters away from the survey line. Lightning effects are included in the analysis for Figure 24 (they are not tagged as outliers) and excluded for Figure 25 (they are tagged as outliers and removed). The apparent resistivities and phases are shown in Figure 26 for the case when the outliers are removed. The response represents significant improvement over our initial robust analysis of the data.

Significant improvements in the robust code are: (1) smooth estimate of the transfer function based on a least squares spline fit to the band averaged estimates. The smooth estimate is used for estimating the residuals that are then used to detect and remove outliers in the time domain and to estimate the frequency domain whitening and weights, (2) section weights based on coherence, signal/noise level and discrepancy of the transfer function from its median value for both the entire frequency range and by frequency bands, and (3) smooth estimates excluding band estimates having low coherence or large errors. This eliminates the dead band effect on the smooth estimates.

The robust method depends on correcting the time series for the filters using a spline interpolation between the measurement filter response. This interpolation did not work well for the present data due to notch filters that cause the filter response to change rapidly in phase with frequency. We found, however, that the ratio of the electric response over the magnetic response is smoothly varying in frequency and can therefore be spline interpolated. Correcting the magnetic series for the ratio of the filters removes the filter effects from the transfer function.
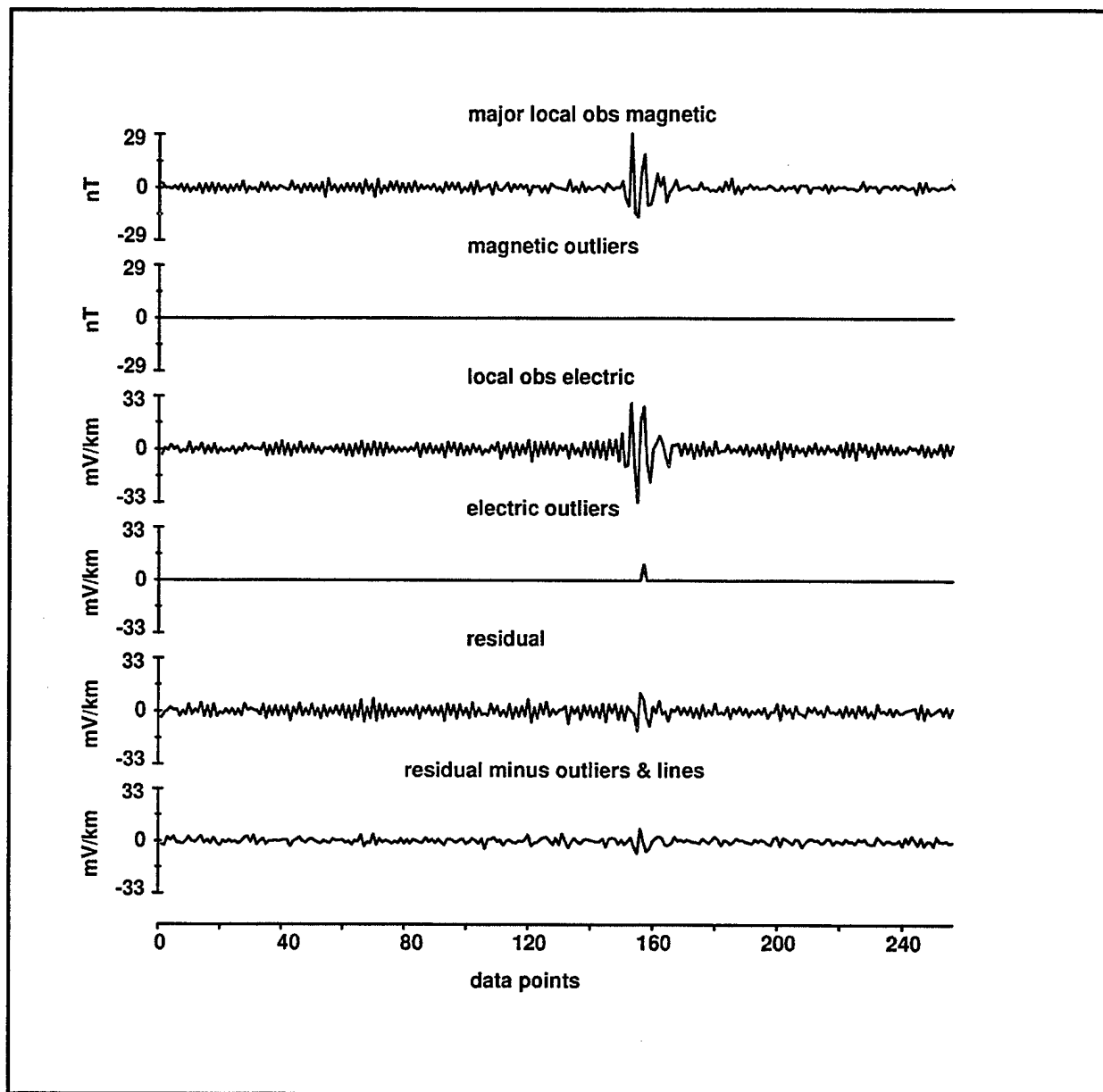
Figure 24. Example of time series containing lightning effects that were included in the determination of the transfer function. The small periodic variations are due to the transmitter.
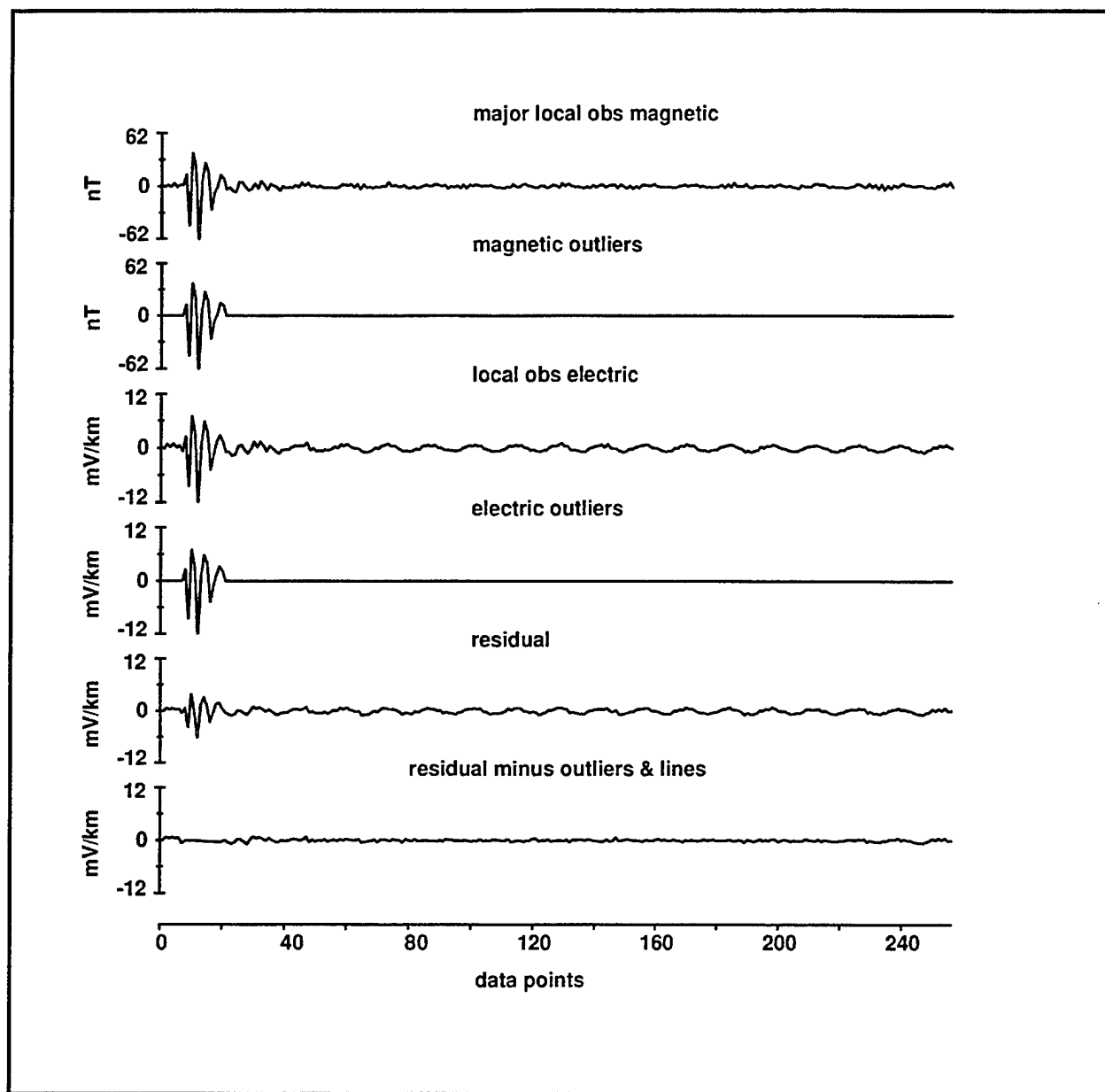
Figure 25. Example of time series containing lightning effects that were excluded from the analysis.
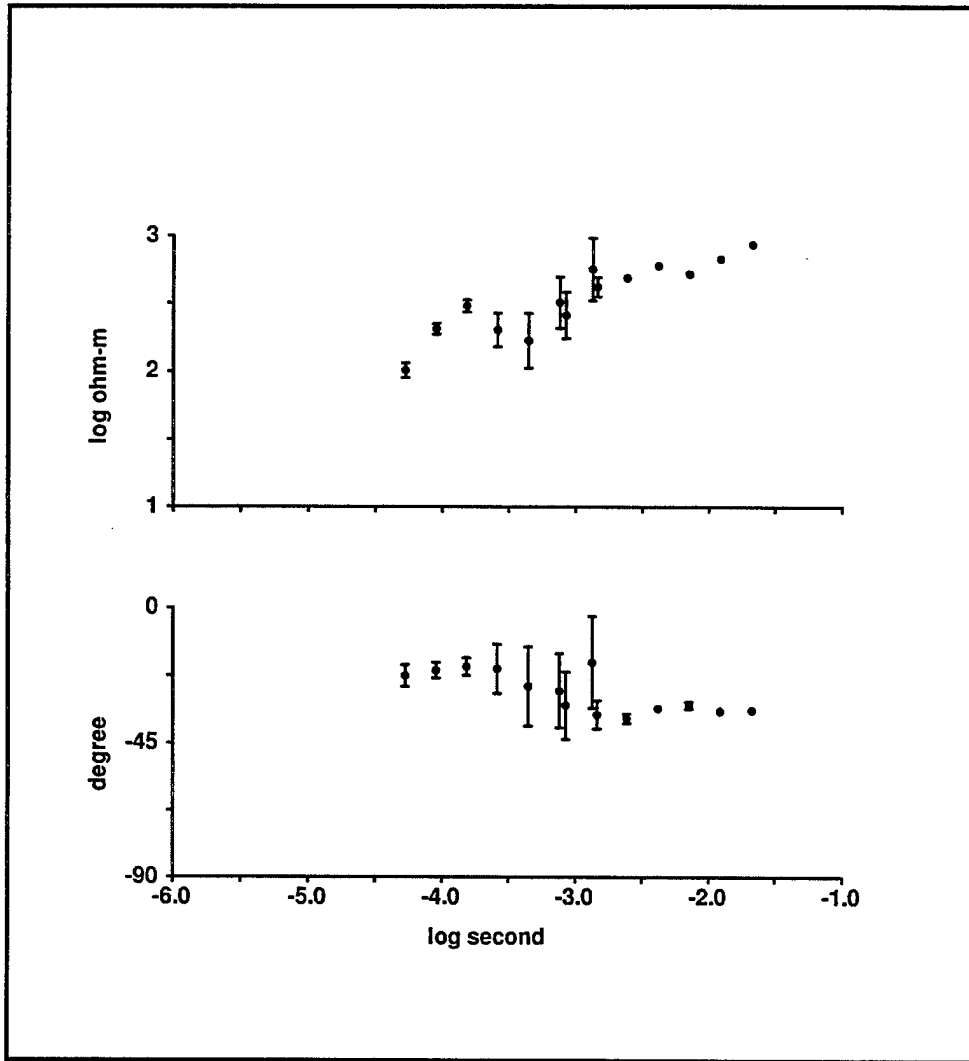
Figure 26. Transfer function for the -Zen element. Note that the high and low band estimates fit nicely together.

7. Conclusions

We have reported on our research from a one year contract with the Air Force Research Laboratory for advanced imaging of underground structure using HAARP. Our research has included the following areas: 1) adaptation of our minimum structure inversion algorithms to solve for simple parametric models, 2) analysis of the sensitivity and resolution of surface EM data to subsurface tunnels, 3) analysis of EM data collected independently over known tunnels, and 4) modification of our robust processing algorithms to deal with AMT data and controlled source transmitters. Our parametric inversion algorithms include one to invert for sharp

boundaries of variable geometry and one that inverts for a rectangular body in a background media. Both have proven successful for simple models. Our analysis of sensitivity and resolution of surface EM data indicates that tunnels need to be at depth to diameter ratios of approximately 3:1 in order to be detectable by surface EM methods. This was borne out by analysis of actual field data, all of which was of marginal quality. Low signal levels and noise resulted in noisy and biased data, making accurate interpretations difficult. We have modified our robust processing algorithms to deal with AMT data and controlled sources, with a resulting improvement in the responses in cases of low signals and high noise levels.

References

Constable, S.C., Parker, R.L., and Constable, C.G., 1987, Occam's inversion: A practical algorithm for generating smooth models from electromagnetic sounding data, *Geophysics, 52*, 289–300.

deGroot-Hedlin, C., and Constable, S., 1990, Occam's inversion to generate smooth, two-dimensional models from magnetotelluric data, *Geophysics, 55*, 1613–1624.

Ellis, R.G. and Oldenburg, D.W., 1994, The pole-pole 3-D DC-resistivity inverse problem: a conjugate gradient approach, *Geophys. J. Int., 119*, 187–194.

Jiracek, G.R., Rodi, W.L., and Vanyan, L.L., 1987, Implications of magnetotelluric modeling for the deep crustal environment in the Rio Grande rift, *Phys. Earth Planet. Interiors, 45*, 179–192.

Larsen, J.C., Mackie, R.L., Manzella, A., Fiordelisi, A., and Rieven, S., 1996, Robust smooth MT transfer functions, *Geophys. J. Int., 124*, 801–819.

Mackie, R.L., and Madden, T.R., 1993, Three-dimensional magnetotelluric modeling using conjugate gradients, *Geophys. J. Int., 115*, 215–229.

Mackie, R.L., Smith, J.T., and Madden,T.R., 1994, Three-dimensional electromagnetic modeling using finite difference equations: The magnetotelluric example, *Radio Science, 29*, 923–935.

Madden, T.R., 1972. Transmission systems and network analogies to geophysical forward and inverse problems, *ONR Tech. Rep., 72-3*.

Madden, T.R., and Mackie, R.L., 1989, Three-dimensional magnetotelluric modeling and inversion, *Proc. IEEE, 77*, 318–333.

Newman, G., 1995, Crosswell electromagnetic inversion using integral and differential equations, *Geophysics, 60*, 899–911.

Park, S.K., and Van, G.P., 1991, Inversion of pole-pole data for 3-D resistivity structure beneath arrays of electrodes, *Geophysics, 56*, 951–960.

Portniaguine, O., and Zhdanov, M.S., 1995, Parameter estimation method in the solution of multi-dimensional geo-electromagnetic inverse problems, *Intl. Symposium on Three-Dimensional Electromagntics*, Schlumberger-Doll Research, pp. 397–403.

Rodi, W.L., 1976, A technique for improving the accuracy of finite element solutions for magnetotelluric data, *Geophys. J. R. astr. Soc., 44*, pp. 483–506.

Rodi, W.L., 1989, Regularization and Backus-Gilbert estimation in nonlinear inverse problems: application to magnetotellurics and surface waves, *PhD Thesis*, Pennsylvania State University, University Park.

Rodi, W.L., and Mackie, R.L., 1999, Nonlinear conjugate gradients for two-dimensional magnetotelluric inversion, accepted by *Geophysics*.

Smith, J.T., and Booker, J.R., 1988, Magnetotelluric inversion for minimum structure, *Geophysics, 53*, 1565–1576.

Smith, J.T., and Booker, J.R., 1991, Rapid inversion of two- and three-dimensional magnetotelluric data, *J. Geophys. Res., 96*, 3905–3922.

Tarantola, A., 1987, *Inverse problem theory*, Elsevier.

Tikhonov, A.N. and Arsenin, V.Y., 1977, *Solutions of Ill-Posed Problems*, V.H. Winston and Sons, Washington. D. C.

Vozoff, K., 1991, The magnetotelluric method, in *Electromagnetic Methods in Applied Geophysics*, edited by M. N. Nabighian, pp. 641–711, Society of Exploration Geophysics, Tulsa, Okla.

Wannamaker, P.E., Hohmann, G.W., and Ward, S.H., 1984, Magnetotelluric responses of three-dimensional bodies in layered earths, *Geophysics, 49*, 1517–1534.

Zhang, J., Mackie, R.L., and Madden, T.R., 1995, Three-dimensional resistivity forward modeling and inversion using conjugate gradients, *Geophysics, 60*, 1313–1325.